



**MSc in Management - Business Analytics**

*Academic Thesis*

Academic year 2022 - 2023

**Floods and Death Toll**

Spin off Climate-Related Disasters and Death Toll

**Manunpat Sirijaturaporn**

*Under the supervision of* Professor Valérie Chavez-Demoulin

## Executive summary

This thesis focuses on the intersection of climate change and wealth inequality, particularly in the context of floods. It draws inspiration from Chavez-Demoulin, Jondeau, and Mhalla's work in 2021, highlighting how carbon emissions intensify climate change, resulting in more extreme flood events. Additionally, it explores how GDP per capita shapes flood severity, showing that regions with higher GDP tend to encounter less severe flood events. Utilizing robust quantitative methodologies, particularly the application of Extreme Value Theory encompassing Poisson and Generalized Pareto Distribution (GPD) models, this research draws upon data derived from reputable sources such as EM-DAT, World Bank, and IPCC databases. Based on IPCC scenarios, the projections yield these key observations. (1) Flood Frequency: A positive correlation is evident between flood frequency and CO<sub>2</sub> emissions, with decreasing trends observed across most scenarios, except for SSP5-8.5, characterized by high emissions and pronounced climate system impacts. (2) Average Death per Event: GDP inversely affects flood severity, with higher GDP regions experiencing milder events. Projections highlight severity reduction across scenarios. (3) Annual Deaths: Projections suggest decreased deaths across scenarios except for SSP5-8.5.

Implications span effective risk reduction, early warning systems, and vulnerability research in developing nations. This study enriches climate disaster literature by providing insights into flood management challenges, mitigation, and research paths. Acknowledged limitations include regional classifications, data scarcity, and modeling non-linear vulnerability dynamics. Further research could refine classifications, analyze temporal data variations, and model non-linear income-vulnerability relationships.

## Acknowledgements

I wish to extend my sincere appreciation to Professor Valérie Chavez-Demoulin for her invaluable support throughout my thesis journey. Her understanding and accommodation in light of the family issues I faced at the thesis's commencement were truly remarkable. Professor Chavez-Demoulin's guidance and unwavering encouragement provided me with the necessary conveniences to navigate those challenging times. Her encouragement and assistance allowed me to find solutions while ensuring that my academic pursuits remained on track. The opportunity she provided not only enhanced my skills and connections but also opened doors to meaningful interactions with fellow PhD graduates and professors, enriching both my academic and professional journey.

I extend my appreciation to Professor Eric Jondeau, an esteemed figure in the field of Finance and a renowned faculty member at HEC Lausanne, University of Lausanne, and the Swiss Finance Institute. I am honored to have him as an expert on my defense day, and I am grateful for his valuable insights and contributions to my work.

I am equally thankful to Professor Linda Mhalla, an expert in Statistics from the École Polytechnique Fédérale de Lausanne (EPFL), who has lent her expertise to this thesis. Her guidance and input have added depth and rigor to my research.

Additionally, I am deeply indebted to my family and friends who have provided unwavering support and encouragement throughout this thesis process. Their belief in my abilities has been a driving force are deeply appreciated.

In closing, I would like to acknowledge the pivotal role that my supervisors and mentors have played in shaping the trajectory of this thesis. Their guidance and support have been indispensable, and I am truly grateful for their contributions.

## Contents

Figures	5
Tables	7
1. Introduction and Literature Review	9
2. Data	15
2.1 Disaster-related data . . . . .	15
2.2 Region Classification . . . . .	16
2.3 Historical covariates data . . . . .	19
2.4 Covariates projections . . . . .	23
2.5 Exploratory Data Analysis . . . . .	31
3. Methodology and Modelling	42
3.1 Poisson distribution . . . . .	42
3.2 Generalized Pareto distribution . . . . .	43
3.3 Flow chart diagram . . . . .	48
4. Results	51
4.1 Frequency . . . . .	51
4.2 Severity . . . . .	54
4.3 Annual Deaths . . . . .	60
4.4 World . . . . .	61
5. Conclusion, Limitation, and Future Research	65
5.1 Conclusion . . . . .	65
5.2 Limitation . . . . .	66

5.3 Future Research . . . . .	68
Appendix A: Expected Annual Frequency Projections	69
Appendix B: Expected Death toll per event Projections	71
Appendix C: Annual Death Projections	73
Bibliography	75

## Figures

1	Distribution of Disasters by Type (1900-2023) . . . . .	10
2	Number of Deaths by Disaster Type (1900-2023) . . . . .	11
3	Annual Frequency of Flood Events (1900-2022) . . . . .	11
4	Average Mortality per Flood Event in log scale (1900-2022) . . . . .	12
5	Shared Socio-economic Pathways and year 2100 radiative forcing combinations [11] . . . . .	27
6	Annual Frequency of Flood event per region (1960-2020) . . . . .	32
7	CO <sub>2</sub> emissions per capita (1960-2020) . . . . .	33
8	Correlation CO <sub>2</sub> emissions per capita and Number of Flood per region (1960-2020) . . . . .	34
9	Average deaths per flood in log scale (1960-2020) . . . . .	36
10	GDP per capita each region (1960-2020) . . . . .	36
11	Correlation between GDP per capita and Average Deaths per flood (1960-2020) . . . . .	37
12	Total Deaths . . . . .	38
13	CO <sub>2</sub> Emissions per Capita Projections in the 5 Scenarios . . . . .	39
14	GDP per Capita Projections . . . . .	41
15	Exponential QQ plot of flood data . . . . .	44
16	Flowchart Illustrating Parameter Estimation for Poisson Distribution and Generalized Pareto Distribution (GPD) . . . . .	50
17	Frequency of Flood from 1960 to 2020. The black line represents the actual data, the red line denotes the expected frequency from the model, and the blue and green lines represent the lower and upper bounds of the 95% confidence interval, respectively. . . . .	53

18	Scatter Plot Comparing Actual Flood Frequency with Model-Estimated Expected Frequency . . . . .	54
19	Projections of Frequency of Flood (all scenarios) . . . . .	55
20	Average death per flood event from 1960 to 2020. The black line repre- sents the actual data, the red line denotes the expected death per flood event from the model, and the blue and green lines represent the lower and upper bounds of the 95% confidence interval, respectively. . . . .	57
21	Scatter Plot Comparing Actual Severity per flood event with Model- Estimated Severity . . . . .	58
22	Projection number of death per flood event in 2030, 2040, and 2050 . . . . .	59
23	Projection annual death in 2030, 2040, and 2050 . . . . .	60
24	Projected Global Flood Frequency in 2030, 2040, and 2050 with 95% Confidence Interval . . . . .	62
25	Projected Global Death per flood incident in 2030, 2040, and 2050 with 95% Confidence Interval . . . . .	63
26	Projected Total Annual Global Deaths for 2030, 2040, and 2050 with a 95% Confidence Interval . . . . .	64

## Tables

1	IIASA-IPCC 5 Regions . . . . .	17
2	IIASA-IPCC 6 Regions . . . . .	17
3	IIASA-IPCC 10 Regions . . . . .	18
4	Mapping Regions . . . . .	19
5	Shared Socioeconomic Pathways in the IPCC Sixth Assessment Report . . .	28
6	Total Number of Floods per Region from 1960 to 2020 . . . . .	32
7	Average Deaths per Flood each region . . . . .	35
8	Parameter estimation ( $\lambda$ ) of the Poisson-Frequency model: *** p<0.001, ** p<0.01, * p<0.05 . . . . .	52
9	Parameter estimation ( $\nu$ ) of the GPD-Severity model: *** p<0.001, ** p<0.01, * p<0.05 . . . . .	56
10	Parameter estimation ( $\xi$ ) of the GPD-Severity model: *** p<0.001, ** p<0.01, * p<0.05 . . . . .	56
A1	Expected Annual Flood Frequency Projections - SSP1-1.9 . . . . .	69
A2	Expected Annual Flood Frequency Projections - SSP1-2.6 . . . . .	69
A3	Expected Annual Flood Frequency Projections - SSP2-4.5 . . . . .	69
A4	Expected Annual Flood Frequency Projections - SSP3-7.0 . . . . .	70
A5	Expected Annual Flood Frequency Projections - SSP5-8.5 . . . . .	70
B1	Expected Death toll per event Projections - SSP1-1.9 and SSP1-2.6 . . . .	71
B2	Expected Death toll per event Projections - SSP2-4.5 . . . . .	71
B3	Expected Death toll per event Projections - SSP3-7.0 . . . . .	71
B4	Expected Death toll per event Projections - SSP5-8.5 . . . . .	72

C1	Expected Annual Death Projections - SSP1-1.9 . . . . .	73
C2	Expected Annual Death Projections - SSP1-2.6 . . . . .	73
C3	Expected Annual Death Projections - SSP2-4.5 . . . . .	73
C4	Expected Annual Death Projections - SSP3-7.0 . . . . .	74
C5	Expected Annual Death Projections - SSP5-8.5 . . . . .	74

## 1. Introduction and Literature Review

This thesis explores the urgent issues of climate change and wealth inequality and their complex implications for global disasters. The inspiration for this study stems from the work on Climate-Related Disasters and Death Toll (2021), authored by Valérie Chavez-Demoulin, Eric Jondeau, and Linda Mhalla [2]. It is widely recognized that carbon emissions, primarily from human activities, contribute to global warming and climate change. According to the IPCC 2023 report [8], climate change is currently impacting various weather and climate extremes worldwide. It highlights that as global warming intensifies, the losses and damages caused by climate change also increase. In addition, there is growing evidence indicating that climate change, including the rise of global temperatures and changes in precipitation patterns, is directly impacting the frequency, and duration of disasters. Additionally, these disasters seem to hit harder in places where the average income (GDP per capita) is lower. According to UNDRR [5], over the last half-century, the least developed countries, despite contributing to only about 1% of global emissions and experiencing only close to 20% of the total number of global disasters, have tragically accounted for almost 70% of the deaths caused by climate-related disasters. This paper aims to examine the connection between carbon emissions and how often disasters happen, as well as the link between a country's average income and how severely a disaster impacts it.

Figure 1 depicting the most frequent disaster types (1900-2023) using data from The Emergency Events Database (EM-DAT) [12]: The chart showcases the prevalence of various disaster types observed between 1900 and 2023. *Flood* emerges as the most frequent disaster with a total of 5,778 occurrences, followed closely by *Storm* with 4,601 occurrences. The number of *Earthquakes* (1,588) and *Epidemics* (1,514) are slightly similar, as are *Droughts* (801) and *Landslides* (801). The substantial disparity between the frequencies of floods and storms compared to other disasters highlights their significant impact on global disaster events.

Figure 2 presents the total number of deaths attributed to each disaster type from 1900 to 2023 [12]. The chart vividly showcases the mortality counts for each disaster category during this period. Remarkably, *Drought* emerges as the primary cause, accounting for nearly

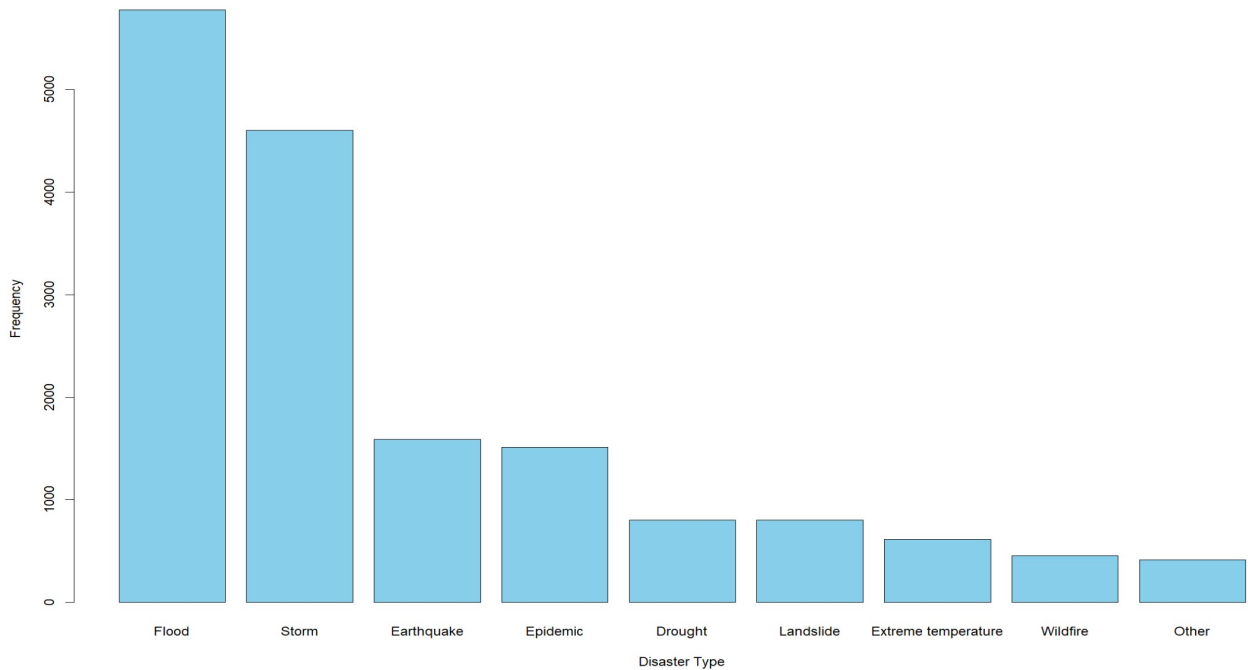


Figure 1. Distribution of Disasters by Type (1900-2023)

12 million deaths, followed by *Epidemic* with 9.6 million deaths and *Flood* with 7 million deaths. Subsequently, the remaining disaster types exhibit significantly lower mortality rates compared to the top three. It is noteworthy that each vertical bar represents the number of deaths per disaster type, scaled to units of 100,000 deaths.

Considering that floods rank highest in terms of occurrence and third in terms of fatality rates, it is evident that they present a significant global issue, warranting our focused attention in this thesis. However, it is important to note that while our models focus on floods, the methodologies can also be applied to other types of disasters.

In Figure 3, we analyse the annual global frequency of floods spanning the years 1900 to 2022. Our findings illustrate a significant increase in flood occurrences, particularly after the mid-20th century, from an estimated 10 floods annually in 1950, surging to exceed over 100 floods annually by the year 2000. It is important to note that one possible explanation for the seemingly lower frequency of events in the earlier part of the 20th century may be attributed to reporting bias. This is because historical disaster records might be limited, potentially leading to a skewed representation. It is possible that only the most severe

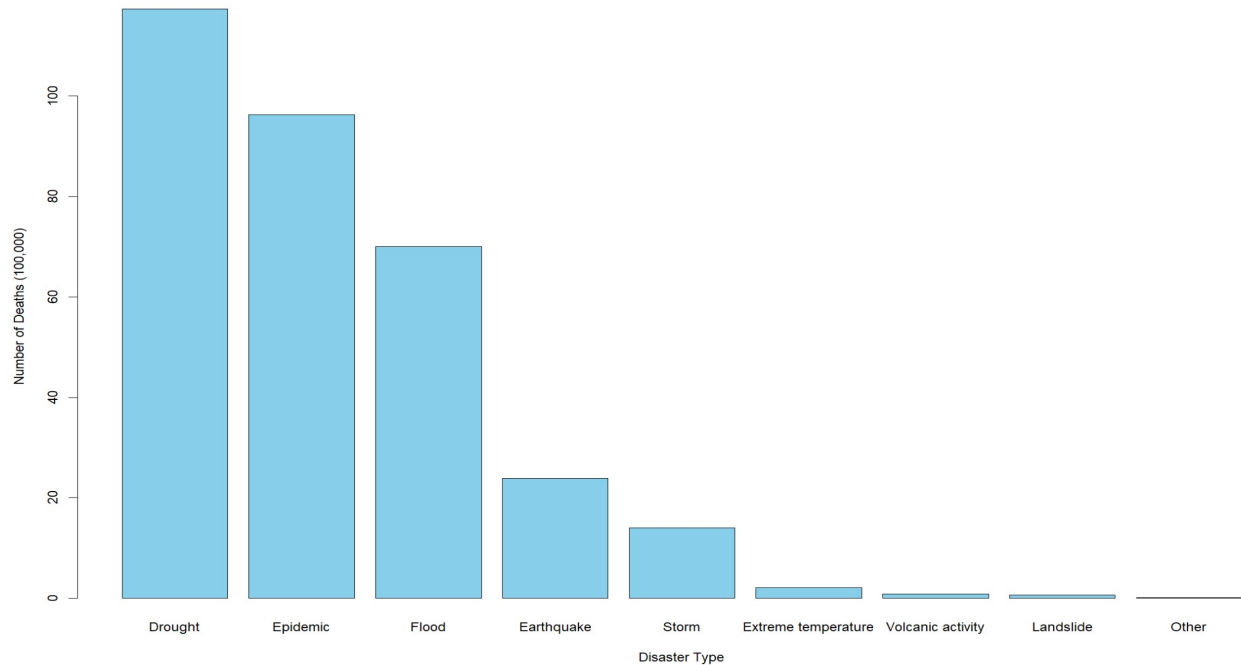


Figure 2. Number of Deaths by Disaster Type (1900-2023)

occurrences were recorded, thereby contributing to a potential underestimation of flood events in the past.

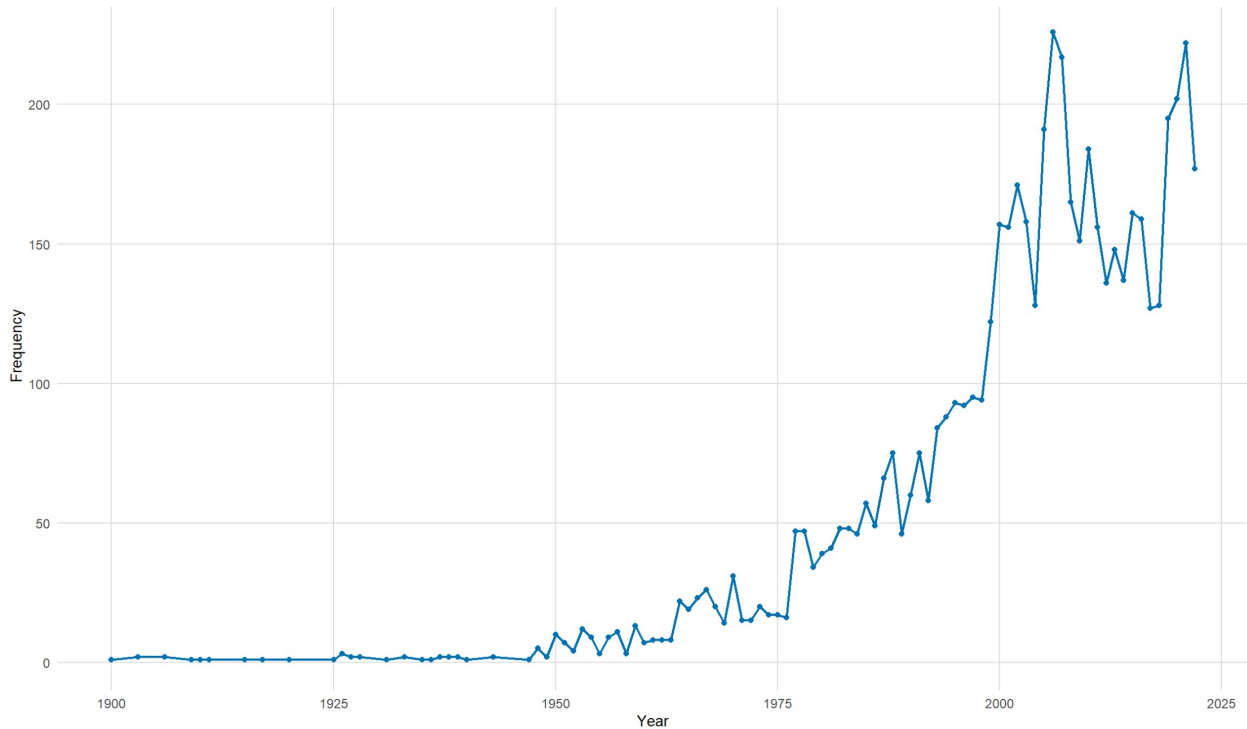


Figure 3. Annual Frequency of Flood Events (1900-2022)

In Figure 4, we can observe the average number of fatalities per flood event (on a logarithmic scale), indicating a downward trend over time. Back in 1950, the recorded number of fatalities per flood event fluctuated between an Expected 100 to 1,000. However, at present, the figures have significantly reduced to less than 100 fatalities per event on average. This reduction in fatalities may be attributed to advancements in disaster risk management strategies implemented over the years.

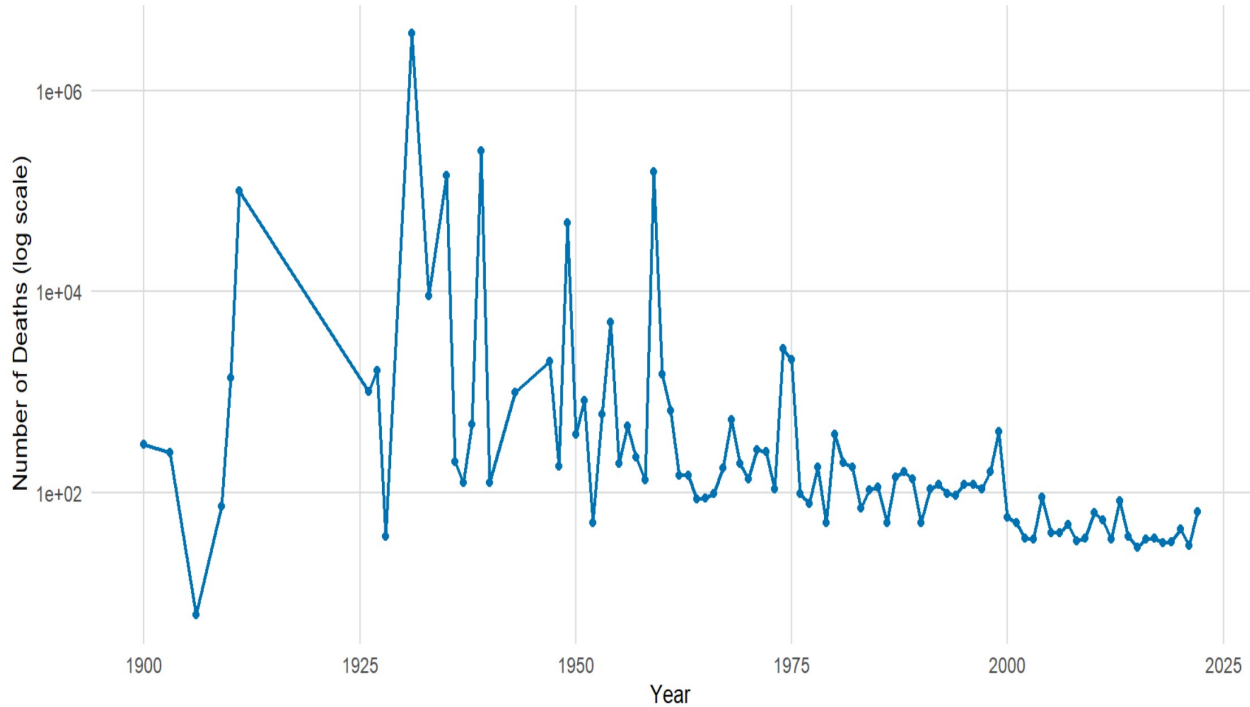


Figure 4. Average Mortality per Flood Event in log scale (1900-2022)

It is clear that both the frequency of floods and the loss severity are not stationary. Our hypothesis is that the increase in flood frequency, to some extent, is attributable to climate change. Furthermore, we contend that the severity of floods is influenced by two primary factors. First, an escalating population inherently heightens the potential death toll due to a larger pool of individuals susceptible to floods. Second, a rise in national income often correlates with the development of superior infrastructure and enhanced disaster risk management strategies, which in turn, tend to mitigate the number of fatalities resulting from such disasters, as floods.

We aim to develop two statistical models that can forecast the frequency and severity of floods based on the covariates.

One of the models relates flood frequency to climate change, particularly to CO<sub>2</sub> emissions. According to the IPCC report [3], greenhouse gas (GHG) emissions, including carbon dioxide (CO<sub>2</sub>), have increased the atmospheric concentrations of several GHGs, such as CO<sub>2</sub>, methane (CH<sub>4</sub>), nitrous oxide (N<sub>2</sub>O), which have resulted in global warming and alterations in the global water cycle, including its variability, global monsoon precipitation, and extreme wet and dry weather and climate events and seasons. These changes in extremes become more pronounced with every additional degree of global warming. Furthermore, Vinod Thomas et al. [15] reported a significant association between climate-related hazards (e.g. rainfall and temperature) and the disaster frequency in Asia-Pacific. Therefore, we use CO<sub>2</sub> emission per capita as a covariate to explain the disaster frequency, as it reflects the contribution of human activities to climate change and its impacts.

The second model associates the flood severity in a specific region with the GDP per capita of that region. Several studies examine the relationship between a country's development level and the extent to which the country suffers from disasters. For instance, World Bank [7] reported that, from 1970 to 2019, 91 percent of all deaths from weather, climate, and water hazards occurred in developing economies. The lower the income level of a community, the more susceptible it is to natural hazards and climate change. In addition, Centre for Research on the Epidemiology of Disasters and UN Office for Disaster Risk Reduction [13] studied the EM-DAT data and found that low and middle-income countries have much higher exposure to disasters and mortality risk, which requires improved early warning systems, better preparedness, weather forecasting and more investment in resilient infrastructure. To account for the variation in development levels and vulnerability across regions, in this paper, we use GDP per capita per region as a covariate in our analysis of the death per event from disasters. However, we acknowledge that this relationship might not be linear, as suggested by Thomas et al [15]. They argued that income levels have a non-linear effect on vulnerability. Specifically, they contended that higher income per capita initially increases the exposure and susceptibility of the population to natural disasters due to inadequate natural disaster management, particularly in developing countries that prioritize

economic growth. However, as time progresses, this vulnerability diminishes as economies and individuals strengthen their capacity and resilience, leading to a reduction in the risk of being affected by natural disasters. In this paper, we do not explore this non-linear effect further.

Then, we employ our models and the projections of carbon emission, gross domestic product (GDP), and population from the Intergovernmental Panel on Climate Change (IPCC) and the Shared Socioeconomic Pathways (SSP). These projections present different SSP scenarios that reflect the potential consequences of human actions on the climate system. By using these projections, we can simulate the frequency and severity of floods under various climate change scenarios. Then, we combine the simulated flood outcomes with the projected population data to estimate the expected death toll due to floods in different regions and time periods.

The paper is structured as follows: In Section 2, we provide an overview of the data used in our empirical analysis. Subsequently, in Section 3, we describe the methodology employed for modeling both the frequency and severity of floods. In section 4, we present the projections for the frequency of floods in the years 2030, 2040, and 2050, along with the corresponding number of deaths per flood event and the total deaths in each of those years. Finally, in Section 5, we conclude the paper and engage in discussions of some potential issues arising from our approach and possible further study.

## 2. Data

### 2.1 Disaster-related data

One of the critical resources of this research paper is EM-DAT, the Emergency Events Database, a comprehensive data repository that captures and documents the occurrence and consequences of over 26,000 mass disasters that have occurred worldwide from 1900 to the present day. The Centre for Research on the Epidemiology of Disasters (CRED) and the World Health Organization (WHO) created EM-DAT through a collaborative effort in 1988. This extensive database is a culmination of information collected from various authoritative sources, including UN agencies, non-governmental organizations, reinsurance companies, research institutes, and press agencies [12].

The primary objective behind the creation and maintenance of EM-DAT is to facilitate humanitarian action at both national and international levels. The database plays a vital role in supporting decision-making processes related to disaster preparedness and the formulation of strategies for disaster risk reduction. Additionally, it serves as an unbiased and reliable foundation for conducting vulnerability assessments and establishing priorities in disaster management.

EM-DAT applies specific inclusion criteria to ensure that its focus is on significant disasters. The database captures human and economic losses at the country level for disasters that meet at least one of the following criteria:

- Fatality Count: The disaster resulted in at least 10 fatalities.
- Affected Population: The disaster affected a minimum of 100 people.
- State of Emergency: A formal declaration of a state of emergency was issued in response to the disaster.
- International Assistance: The occurrence of the disaster prompted a call for international assistance to manage the situation effectively.

EM-DAT provides detailed information on various aspects of each disaster, such as the fatality count, the number of affected individuals, the financial losses in U.S. dollars, and the insured losses in U.S. dollars, from 1900 to 2023. This data is categorized by year,

region, and country. Furthermore, the database classifies natural disasters into 14 distinct types such as earthquakes, floods, droughts, extreme temperatures, landslides, and storms.

In this thesis, our focus is specifically on floods, and we have chosen to analyse the period from 1960 to 2020. This time frame was selected to mitigate potential reporting bias, as historical records of disasters tend to become less abundant as we delve further into the past. This scarcity can be attributed to the deliberate documentation of only the most severe events. Furthermore, it should be noted that the reported numbers of deaths may be subject to revision or even exclusion in certain cases. Given the extensive duration of the study period, we have addressed the issue of comparability in the number of deaths over time by accounting for changes in a country's population. Thus, we introduce adjustments to the number of deaths caused by event  $i$  in country  $c$  and year  $t$ . We define the rescaled number of deaths as

$$\tilde{D}_{i,t} = D_{i,t} \times \frac{P_T^c}{P_t^c} \quad (1)$$

where  $D_{i,t}$  represents the actual number of deaths during event  $i$  in year  $t$ ,  $P_t^c$  is the population of country  $c$  in year  $t$ <sup>1</sup>, and  $T$  is the year 2020 [2].

## 2.2 Region Classification

The data sources for this study comprise the datasets provided by the International Institute for Applied Systems Analysis (IIASA) as part of a cooperation agreement with Working Group III of the Intergovernmental Panel on Climate Change (IPCC) [14] and the World Bank Open Data. In the forthcoming sections of this paper, we will provide detailed explanations and analyses of these datasets, shedding light on their significance and relevance to our research.

---

1. The World Bank Open Data code SP.POP.TOTL (Population, total) provides the yearly population data for countries from 1960 to 2021 (updated on June 29th, 2023).

The World Bank data is classified into seven regions, namely East Asia & Pacific, Europe & Central Asia, Latin America & Caribbean, Middle East & North Africa, North America, South Asia, and Sub-Saharan Africa.<sup>2</sup>

On the other hand, the IIASA-IPCC data is publicly available for download and classified into four region categories: World, R5, R6, and R10 (updated version 1.1). The below tables provide specific details for each category, except for the World category, as it encompasses only one region.<sup>3</sup>

Table 1. IIASA-IPCC 5 Regions

Region code	Definition
R5ASIA	Asian countries except Japan
R5LAM	Latin American countries
R5MAF	Countries of the Middle East and Africa
R5OECD90+EU	OECD90 and EU (and EU candidate) countries
R5REF	Countries from the Reforming Economies of the Former Soviet Union

Table 2. IIASA-IPCC 6 Regions

Region code	Definition
R6AFRICA	Countries of Africa (R6)
R6ASIA	Asian countries except Japan (R6)
R6LAM	Latin American countries (R6)
R6MIDDLE_EAST	Countries of the Middle East (R6)
R6OECD90+EU	OECD90 and EU (and EU candidate) countries (R6)
R6REF	Countries from the Reforming Economies of the Former Soviet Union (R6)

Our analysis aimed for the highest level of regional granularity, leading us to consider the use of IIASA-IPCC classification, specifically the R10 (10 regions) classification. R10

2. For a visual representation of 7 regions, a map can be accessed at the following link: <https://datatopics.worldbank.org/world-development-indicators/the-world-by-income-and-region.html>.

3. The data can be downloaded, and further information regarding the regions and their definitions can be accessed at the provided link under the Download section and the Documentation section respectively: <https://data.ece.iiasa.ac.at/ar6/>.

Table 3. IIASA-IPCC 10 Regions

Region code	Definition
R10AFRICA	Countries of Africa
R10CHINA+	Countries of centrally-planned Asia; primarily China
R10EUROPE	N/A
R10INDIA+	Countries of South Asia; primarily India
R10LATIN_AM	Countries of Latin America and the Caribbean
R10NORTH_AM	North America; primarily the United States of America and Canada
R10MIDDLE_EAST	Countries of the Middle East; Iran, Iraq, Israel, Saudi Arabia, Qatar, etc
R10PAC_OECD	Pacific OECD
R10REF_ECON	Reforming Economies of Eastern Europe and the Former Soviet Union; primarily Russia
R10REST_ASIA	Other countries of Asia

offered the most detailed breakdown and the most appropriate categorization in terms of geographical location and income level among the available region categories.

However, a notable disparity arose when comparing the region definitions between the World Bank dataset and the IPCC R10 dataset. In contrast to the World Bank classification, which makes a clear distinction between North Africa and Sub-Saharan Africa, the IPCC R10 classification lacks a separate designation for these regions within the Africa region. Furthermore, the World Bank classification combines East Asia & Pacific regions, while the IPCC R10 dataset provides a more detailed breakdown. Similarly, the World Bank merges Europe & Central Asia regions, whereas the IPCC R10 classification offers a more granular categorization.

Given the discrepancies between the World Bank and the IIASA-IPCC R10 classifications, it became imperative to devise our own region classification comprising six distinct regions for the purpose of this study. The specific details of this revised classification are presented in Table 4.

By developing our own region classification as illustrated in the *New Region* column in Table 4, we aim to address the disparity between the World Bank and IIASA-IPCC

Table 4. Mapping Regions

<i>New Region</i> used in this study	World Bank region	
East Asia & Pacific	East Asia & Pacific	R10CHINA+ R10PAC_OECD R10REST_ASIA
Europe & Central Asia	Europe & Central Asia	R10EUROPE R10REF_ECON
Latin America & Caribbean	Latin America & Caribbean	R10LATIN_AM
Middle East & Africa	Middle East & North Africa Sub-Saharan Africa	R10AFRICA R10MIDDLE_EAST
North America	North America	R10NORTH_AM
South Asia	South Asia	R10INDIA+

classifications while ensuring that our analysis captures the unique characteristics of different regions in a meaningful way.

### 2.3 Historical covariates data

In this section, our focus is on the utilization of World Bank Open Data. We incorporate two independent variables, namely CO2 emission per capita and GDP per capita, which play a crucial role in explaining the frequency and severity of flood events, respectively.

The decision to employ World Bank data as our primary data source arises from thorough considerations. While the integration of IIASA-IPCC data is of great importance for projecting the frequency and severity of flood events, as we will discuss in the following section, it is important to acknowledge that the IIASA-IPCC data has some limitations concerning historical coverage. The IIASA-IPCC dataset primarily commences from 2005 and is available at a 5-year frequency, thereby providing relatively less comprehensive historical information than the dataset of the World Bank which is covering a longer period. Also, our main dataset, the Emergency Events Database (EMDAT), spans from 1960 and operates on an annual frequency. To incorporate historical covariate data within our analysis, we rely on the World Bank Open Data as the principal data source.

## CO2 Emissions per Capita

Obtaining historical annual CO2 emissions per capita entails referring to two distinct sources. The first source is the World Bank Open Data, specifically the dataset identified by the code EN.ATM.CO2E.PC (updated on June 29th, 2023). The second source is the data on CO2 and Greenhouse Gas Emissions database by Our World in Data [9]. Both sources measure CO2 emissions per capita in metric tons.

Greenhouse gases (GHGs) present a widespread global challenge. These gases can mix and disperse globally in the Earth's atmosphere, meaning that GHGs released in one region will eventually influence the global climate system, not just the local or regional area. This global mixing is why the whole planet experiences the warming effect of GHGs, commonly referred to as global warming or climate change [10]. Consequently, the extensive dispersion of GHGs implies that emissions from a single country, regardless of its location, can affect not only that specific nation and its immediate neighbors but also contribute to the overall global accumulation of greenhouse gases, exerting consequences on the entire planet. Hence, we opt for utilizing global CO2 emissions per capita instead of regional CO2 emissions per capita.

The World Bank dataset on CO2 emissions per capita spans from 1990 to 2020. Consequently, to account for the missing data from 1960 to 1989, we supplemented the dataset by incorporating CO2 emissions per capita data retrieved from Our World in Data, which covers a broader timeframe from 1750 to 2021. However, we do not use Our World in Data as the primary source in this section due to differences in regional classification between World Bank data and Our World in Data, which may result in inconsistencies when compared to GDP per capita.

## GDP per Capita

GDP per capita (Gross Domestic Product per capita) serves as a key measure to explain the severity of flood events. By assessing the economic prosperity of a region, we gain valuable insights into its capability to mitigate and recover from flood-related damages. A higher GDP per capita may indicate greater financial resources and infrastructure devel-

opment, potentially affecting the severity of flood events and the ability to manage their impacts.

During the data preparation stage, we incorporated two variations of GDP per capita: GDP per capita in constant USD and GDP PPP per capita (Gross Domestic Product per capita adjusted for Purchasing Power Parity) in constant USD. The inclusion of GDP PPP per capita in our analysis is contingent upon the availability of sufficient data.

GDP PPP per capita accounts for Purchasing Power Parities (PPP), which are currency conversion rates designed to equalise the purchasing power of different currencies by adjusting for price level differences between countries. These PPP conversion rates are expressed in terms of national currency per US dollar [6]. On the other hand, GDP per capita is converted by the actual exchange rate. GDP per capita PPP in USD is a better indicator than GDP per capita in USD because it takes into account variations in living costs across different countries. This means that PPP per capita is a measure of the average purchasing power of a country's population, while GDP per capita is a measure of the average income of a country's population. For example, country *A* and country *B* both have a GDP per capita of 10,000 in their respective local currencies. If the exchange rate between the two countries is 1 to 1, one might conclude that both countries have the same level of economic well-being. However, if prices for goods and services are higher in country *A*, then people in country *A* will have lower purchasing power and a lower standard of living than people in country *B*. For instance, if goods and services that cost 1 unit of local currency *B* in country *B* cost 1.2 units of local currency *A* in country *A*, then the PPP conversion rate will be 1.2 to 1. This means that the GDP per capita PPP of country *A* is 20% lower than that of country *B*. This shows how GDP per capita PPP adjusts for price differences and gives a more accurate comparison of economic well-being.

In the next section, the GDP PPP (in constant 2010 USD) provided by IIASA-IPCC will hold substantial significance in the projection process. To ensure the coherence and uniformity of our data sources, we have employed the GDP PPP per capita values sourced

from the World Bank.<sup>4</sup> It is important to note that the World Bank data is only available in constant 2017 USD and is aggregated at a regional level, encompassing seven distinct regions. In order to maintain consistency with the temporal coverage (from 1960 to 2020) of our main dataset, the Emergency Events Database (EMDAT), a challenge arises due to the absence of World Bank's GDP PPP per capita data (in constant 2017 USD) for the years 1960 to 1989. To address this disparity, we sought an alternative dataset that could provide the necessary coverage. Consequently, we obtained GDP per capita data expressed in 2015 USD, which provides a longer historical coverage commencing from 1960. By applying annual growth rates of GDP per capita (in constant 2015 USD), we were able to retroactively estimate the missing values from 1960 to 1989. However, it should be noted that certain data gaps remained for the Europe & Central Asia region spanning the years 1960 to 1969, as well as for the Middle East & North Africa region spanning the years 1960 to 1974. To overcome these limitations, We employed the GDP per capita figures from 2010, as has been adopted in the previous literature [2]. As a result, our dataset for GDP per capita across the seven regions is complete and spans the period from 1960 to 2020.

Finally, we proceeded to merge the GDP per capita values of the *Middle East & North Africa* region with those of the *Sub-Saharan Africa* region, thereby creating a region named *Middle East & Africa* as outlined in Table 4. We employed the following procedure in the process of the aggregation of GDP per capita:

$$GDP_{t,MEA} = \frac{(GDP_{t,MENA} \times P_{t,MENA}) + (GDP_{t,SA} \times P_{t,SA})}{P_{t,MENA} + P_{t,SA}} \quad (2)$$

where  $GDP_{t,i}$  represents the GDP per capita in year  $t$  of region  $i$ ,  $P_{t,i}$  represents the population in year  $t$  of region  $i$ ,  $MEA$  represents the Middle East & Africa,  $MENA$  represents the Middle East & North Africa,  $SA$  represents Sub-Saharan Africa.

---

4. The World Bank Open Data code NY.GDP.PCAP.PP.KD offers GDP PPP per capita figures (in constant 2017 USD) covering the period from 1990 to 2022 (updated on June 29th, 2023).

## 2.4 Covariates projections

As mentioned previously, the cooperation between the International Institute for Applied Systems Analysis and the Intergovernmental Panel on Climate Change (IIASA-IPCC) is a vital resource in projections of the frequency and severity of flood events. Similar to the historical covariates data section, the two variables of interest, namely CO<sub>2</sub> emissions per capita and GDP per capita, are included in the analysis.

The International Panel on Climate Change (IPCC), established by the United Nations and the World Meteorological Organization, significantly bolsters its credibility as an international organization. By offering policymakers impartial scientific evaluations of climate change risks and impacts, the IPCC serves as a crucial source of reliable information for informed decision-making. Through a rigorous process involving expert input and multiple drafting rounds, the IPCC ensures comprehensive and objective assessments. Its reports reflect diverse scientific perspectives and varying degrees of certainty. With three working groups and a task force focusing on different aspects of climate change, the IPCC produces special reports and methodology reports for targeted assessments and practical guidelines [4].

The International Institute for Applied Systems Analysis (IIASA) is an independent, international research organization that addresses global challenges through interdisciplinary scientific research, focusing on areas like energy, climate change, food security, and policy analysis [1]. IIASA's collaboration with the Intergovernmental Panel on Climate Change (IPCC) plays a crucial role in providing scientific insights and data for IPCC's climate change assessments. IIASA's expertise in systems analysis and policy analysis complements the IPCC's work, ensuring that their assessment reports are based on robust scientific evidence and offering a comprehensive understanding of the global impacts of climate change. This partnership enhances the foundation of IPCC reports, assisting policymakers in making informed decisions to tackle climate change and work towards a sustainable future.

## Five selected scenarios

The Shared Socioeconomic Pathways (SSPs) are a set of scenarios that describe different plausible future socioeconomic developments. These pathways serve as a vital framework for exploring a wide spectrum of potential climate and socioeconomic outcomes that may emerge in the coming years. Through descriptive narratives, the SSPs outline alternative socio-economic developments, offering insights into potential future worlds based on key assumptions concerning population growth, economic advancements, technological innovations, energy consumption, and societal values. It is important to note that the SSPs themselves do not encompass specific datasets; rather, they provide contextual storylines, serving as inputs for various scenarios and model outputs. These scenarios are employed to analyse and assess the potential implications of the SSPs, enabling researchers and policymakers to gain a deeper understanding of the potential trajectories of our global society in the face of evolving socioeconomic and environmental factors.

### ***SSP1: Sustainability - Taking the Green Road (low challenges to mitigation and adaptation)***

- The world shifts gradually, but pervasively, toward a more sustainable path, emphasizing more inclusive development that respects perceived environmental boundaries.
- Management of the global commons slowly improves, educational and health investments accelerate the demographic transition, and the emphasis on economic growth shifts toward a broader emphasis on human well-being.
- Driven by an increasing commitment to achieving development goals, inequality is reduced both across and within countries.
- Consumption is oriented toward low material growth and lower resource and energy intensity.

### ***SSP2: Middle of the road - (medium challenges to mitigation and adaptation)***

- The world follows a path in which social, economic, and technological trends do not shift markedly from historical patterns.

- Development and income growth proceeds unevenly, with some countries making relatively good progress while others fall short of expectations.
- Global and national institutions work toward but make slow progress in achieving sustainable development goals.
- Environmental systems experience degradation, although there are some improvements and overall the intensity of resource and energy use declines.
- Global population growth is moderate and levels off in the second half of the century.
- Income inequality persists or improves only slowly and challenges to reducing vulnerability to societal and environmental changes remain.

***SSP3: Regional rivalry - A rocky road (high challenges to mitigation and adaptation)***

- A resurgent nationalism, concerns about competitiveness and security, and regional conflicts push countries to increasingly focus on domestic or, at most, regional issues.
- Policies shift over time to become increasingly oriented toward national and regional security issues.
- Countries focus on achieving energy and food security goals within their own regions at the expense of broader-based development.
- Investments in education and technological development decline.
- Economic development is slow, consumption is material-intensive, and inequalities persist or worsen over time.
- Population growth is low in industrialized countries and high in developing countries.
- A low international priority for addressing environmental concerns leads to strong environmental degradation in some regions.

***SSP4: Inequality - A road divided (low challenges to mitigation, high challenges to adaptation)***

- Highly unequal investments in human capital, combined with increasing disparities in economic opportunity and political power, lead to increasing inequalities and stratification both across and within countries.
- Over time, a gap widens between an internationally-connected society that contributes to knowledge- and capital-intensive sectors of the global economy, and a fragmented collection of lower-income, poorly educated societies that work in a labor intensive, low-tech economy.
- Social cohesion degrades and conflict and unrest become increasingly common.
- Technology development is high in the high-tech economy and sectors.
- The globally connected energy sector diversifies, with investments in both carbon-intensive fuels like coal and unconventional oil, but also low-carbon energy sources. Environmental policies focus on local issues around middle and high income areas.

***SSP5: Fossil-fueled development - Taking the highway (high challenges to mitigation, low challenges to adaptation)***

- This world places increasing faith in competitive markets, innovation and participatory societies to produce rapid technological progress and development of human capital as the path to sustainable development.
- Global markets are increasingly integrated.
- There are also strong investments in health, education, and institutions to enhance human and social capital.
- At the same time, the push for economic and social development is coupled with the exploitation of abundant fossil fuel resources and the adoption of resource and energy intensive lifestyles around the world.
- All these factors lead to rapid growth of the global economy, while global population peaks and declines in the 21st century.
- Local environmental problems like air pollution are successfully managed.
- There is faith in the ability to effectively manage social and ecological systems, including by geo-engineering if necessary.

SSP-based scenarios are referred to as SSPx-y, where 'SSPx' refers to the Shared Socioeconomic Pathway describing the socioeconomic trends underlying the scenarios, and 'y' refers to the level of radiative forcing (in watts per square metre, or W m<sup>-2</sup>) resulting from the scenario in the year 2100 [8].

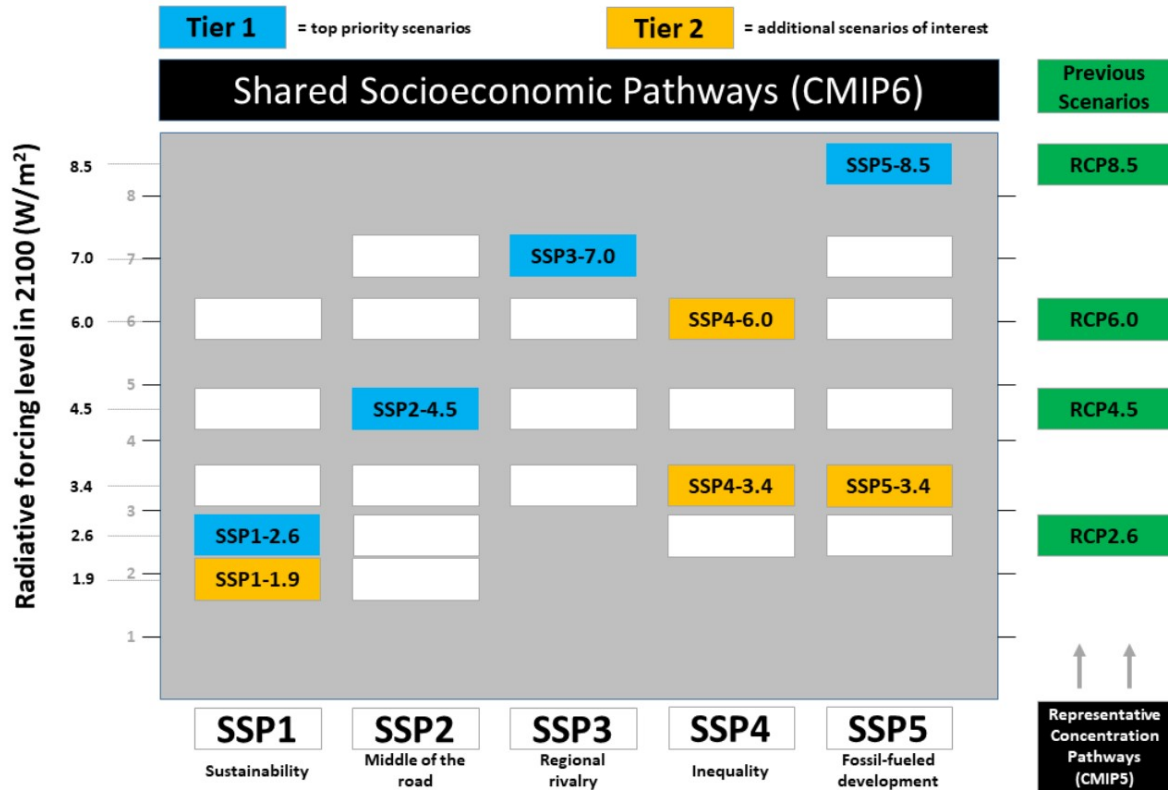


Figure 5. Shared Socio-economic Pathways and year 2100 radiative forcing combinations [11]

The illustration in Figure 5 presents a comprehensive display of potential combinations resulting from the multitude of scenarios. To address the complexity and abundance of these scenarios, certain priority levels were assigned to aid modeling organizations in their selection. Among these scenarios, four scenarios were designated as 'Tier 1' (blue) scenarios, signifying the highest priority for consideration. These Tier 1 scenarios encompass a wide spectrum of uncertainty, capturing various future socio-economic and climate-forcing pathways. In addition to the Tier 1 scenarios, there exist 'Tier 2' (yellow) scenarios, offering additional avenues of interest for modeling centers to explore if available resources allow. The classification into priority tiers facilitates an organized and strategic approach

in understanding and simulating a diverse range of potential futures, thereby enhancing the robustness and applicability of the models.

Our projections rely on the Shared Socioeconomic Pathways (SSPs) as presented in the Sixth Assessment Report [8]. Within this framework, a set of five scenarios was comprehensively evaluated to project temperature outcomes. These five SSPs were thoughtfully selected to cover a diverse range of potential future trajectories of anthropogenic drivers of climate change. Consequently, they were chosen as the primary subjects of comparison in the report, serving as representatives of distinct pathways for climate change. Moreover, they form a foundational basis for assessing the potential impacts of varying levels of greenhouse gas (GHG) mitigation, enabling a comprehensive analysis of the potential climate futures that lie ahead. The chosen five scenarios are presented in Table 5.

Table 5. Shared Socioeconomic Pathways in the IPCC Sixth Assessment Report

SSP	Scenario
SSP1-1.9	very low GHG emissions: CO2 emissions cut to net zero around 2050
SSP1-2.6	low GHG emissions: CO2 emissions cut to net zero around 2075
SSP2-4.5	intermediate GHG emissions: CO2 emissions around current levels until 2050, then falling but not reaching net zero by 2100
SSP3-7.0	high GHG emissions: CO2 emissions double by 2100
SSP5-8.5	very high GHG emissions: CO2 emissions triple by 2075

## CO2 Emissions per Capita

To obtain the CO2 emission per capita projections, the dataset from the IIASA-IPCC for the World region was accessed<sup>5</sup>. This dataset encompassed CO2 emission projections

---

5. The AR6 Scenario Explorer and Database hosted by IIASA under the Downloads section offers the AR6 Scenarios Database World V1.1, variable name Emissions CO2, (updated on November 9th, 2022).

spanning from 2005 to 2100<sup>6</sup>, measured in metric tons of carbon dioxide per year. To derive the CO2 emission per capita projections, the CO2 emission projections were divided by the corresponding World population projections.

Following that, to ensure consistency and alignment with historical data sourced from the World Bank, we undertook a process of data rebasing. The rebasing was performed by applying the following equation to the IPCC data, thereby guaranteeing harmonization with the World Bank data for the year 2020:

$$\widetilde{CO2}_{IPCC,t} = CO2_{IPCC,t} \times \frac{CO2_{WB,2020}}{CO2_{IPCC,2020}} \quad (3)$$

where

$\widetilde{CO2}_{IPCC,t}$  denotes the rebased CO2 emission per capita value for year  $t$  in the IIASA-IPCC dataset

$CO2_{IPCC,t}$  denotes the corresponding CO2 emission per capita value from the IIASA-IPCC original dataset for year  $t$

$CO2_{WB,2020}$  denotes the corresponding CO2 emission per capita value from the World Bank dataset for year 2020

Through Equation 3, the IIASA-IPCC dataset's CO2 emission per capita values were adjusted proportionally based on the ratio of World Bank data for 2020 to the corresponding IIASA-IPCC data for the same year. This critical step harmonized the datasets, allowing for meaningful comparisons and facilitating a comprehensive analysis of projected climate scenarios while remaining anchored to observed values in the year 2020.

---

6. In this study, specific models are selected for each scenario as follows: SSP1-19 and SSP1-26: IMAGE 3.0.1, SSP2-45: MESSAGE-GLOBIOM 1.0, SSP3-7.0: AIM/CGE 2.0, SSP5-8.5: REMIND-MAgPIE 1.5

## GDP per Capita

The projection of GDP per capita for each region in this study utilizes data sourced from the IIASA-IPCC databases<sup>7</sup>. The IIASA-IPCC database provides GDP PPP (in constant 2010 USD) projections at the regional level, covering the time span from 2005 to 2100<sup>8</sup> and measured in billion per year.

To determine the GDP per capita projections for each region, the GDP PPP projections are divided by the corresponding population projections of the respective regions for each year. This calculation allows us to estimate the economic output on a per-person basis, offering valuable insights into the living standards and economic well-being of the population in each region. Nevertheless, as outlined in Table 4, certain IIASA-IPCC regions are required to be aggregated to our customized region classification. For instance, in the Europe & Central Asia region, the GDP PPP projection involves combining data from two IIASA-IPCC sub-regions: Europe and Reforming Economies of Eastern Europe and the Former Soviet Union (R10EUROPE and R10REF\_ECON). The combined GDP PPP is then divided by the sum of their respective populations for each projection year. Similar considerations apply to the East Asia & Pacific region and the Middle East & Africa region, where GDP PPP data for sub-regions must be combined appropriately before calculating GDP per capita. This approach ensures accuracy and consistency in projecting GDP per capita figures for each region, despite the complexities introduced by the regional subdivisions in certain areas.

Similar to the methodology employed for the CO2 Emissions per Capita section, we pursued a data rebasing procedure to maintain consistency with historical data acquired from the World Bank. This vital process involved applying the below equation to the IIASA-IPCC data, ensuring alignment with the World Bank data for the reference year 2020.

7. The AR6 Scenario Explorer and Database hosted by IIASA under the Downloads section offers the AR6 Scenarios Database R10 regions V1.1, variable name GDP PPP, (updated on November 9th, 2022).

8. In this study, the scenarios SSP1-SPA1-19I-LI, SSP1-SPA1-26I-D, and SSP2-SPA2-45I-D are selected in lieu of SSP1-1.9, SSP1-2.6, and SSP2-4.5, as the latter scenarios are not available in the IIASA-IPCC R10 region. These selections, alongside the scenarios SSP3-7.0 and SSP5-8.5, are all aligned with the sole model IMAGE 3.2[16]

$$\widetilde{GDP}_{IPCC,t} = GDP_{IPCC,t} \times \frac{GDP_{WB,2020}}{GDP_{IPCC,2020}} \quad (4)$$

where

$\widetilde{CO2}_{IPCC,t}$  denotes the rebased GDP per capita value for year  $t$  in the IIASA-IPCC dataset

$CO2_{IPCC,t}$  denotes the corresponding GDP per capita value from the IIASA-IPCC original dataset for year  $t$

$CO2_{WB,2020}$  denotes the corresponding GDP per capita value from the World Bank dataset for year 2020

The implementation of the data rebasing technique facilitated a seamless comparison and analysis of the information within the study, ensuring harmonization between the two datasets. The GDP per capita values in the IIASA-IPCC dataset were rescaled using a proportionate adjustment, determined by the ratio of World Bank data for the year 2020 to the corresponding IIASA-IPCC data for the same year. This crucial step effectively aligned the datasets, enabling meaningful comparisons and facilitating a comprehensive analysis of projected climate scenarios while maintaining a strong anchor to observed values in the reference year 2020.

## 2.5 Exploratory Data Analysis

In this section, we will present two main components of the analysis: 1. Exploratory Data Analysis (EDA) of historical flood data, and 2. EDA of projections based on 5 SSP scenarios.

### Exploratory Data Analysis of historical floods

In the following subsection, we present the exploratory data analysis (EDA) of the EM-DAT data, focusing on the frequency of floods from 1960 to 2000. Table 6 displays the total number of floods per region during this period. The East Asia & Pacific region recorded the highest number of floods (1,291), followed by the Middle East & Africa (1,311), Latin America & Caribbean (967), Europe & Central Asia (746), and South Asia (707).

Notably, North America had the lowest flood occurrence with only 220 observed events. It is important to acknowledge this limited data in North America, as it may potentially impact the standard errors when fitting our model for this region.

Table 6. Total Number of Floods per Region from 1960 to 2020

Regions	Number of Floods
East Asia & Pacific	1,291
Europe & Central Asia	746
Latin America & Caribbean	967
Middle East & Africa	1,311
North America	220
South Asia	707

Figure 6 displays the time series of annual flood occurrence frequencies per region. All regions, except North America, exhibit increasing trends. Notably, the Middle East & Africa region has experienced a significant rise in floods over the past five years. However, the trend in North America appears less conclusive.

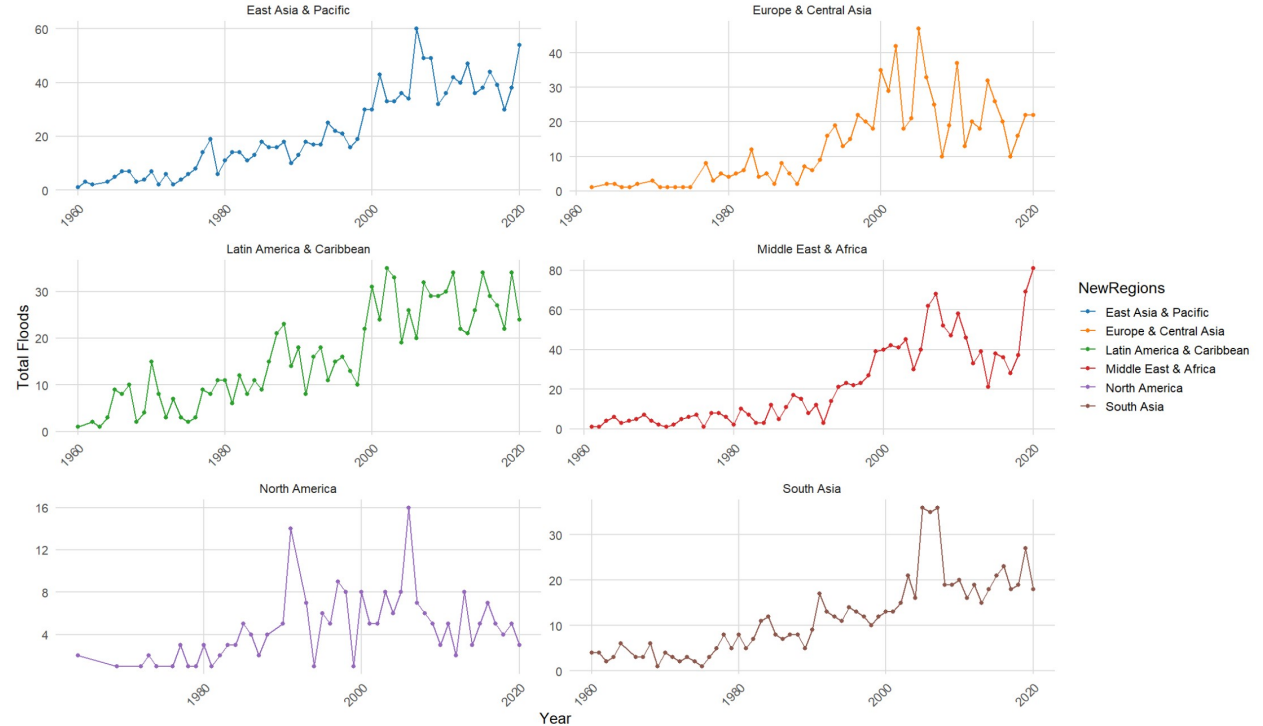


Figure 6. Annual Frequency of Flood event per region (1960-2020)

Figure 7 illustrates the time series of World CO<sub>2</sub> emissions per capita sourced from the World Bank data. Notably, a marked surge in CO<sub>2</sub> emissions is observed during the period from 1960 to 1980, which may be attributed to a rapid boom in oil and gas production during that period. Another substantial upswing is evident in the early 2000s, attributed to the robust economic growth of developing countries, particularly China and India.<sup>9</sup> However, a significant drop in CO<sub>2</sub> emissions is recorded in 2020, largely attributed to the implementation of widespread lockdown measures in response to the COVID-19 pandemic.

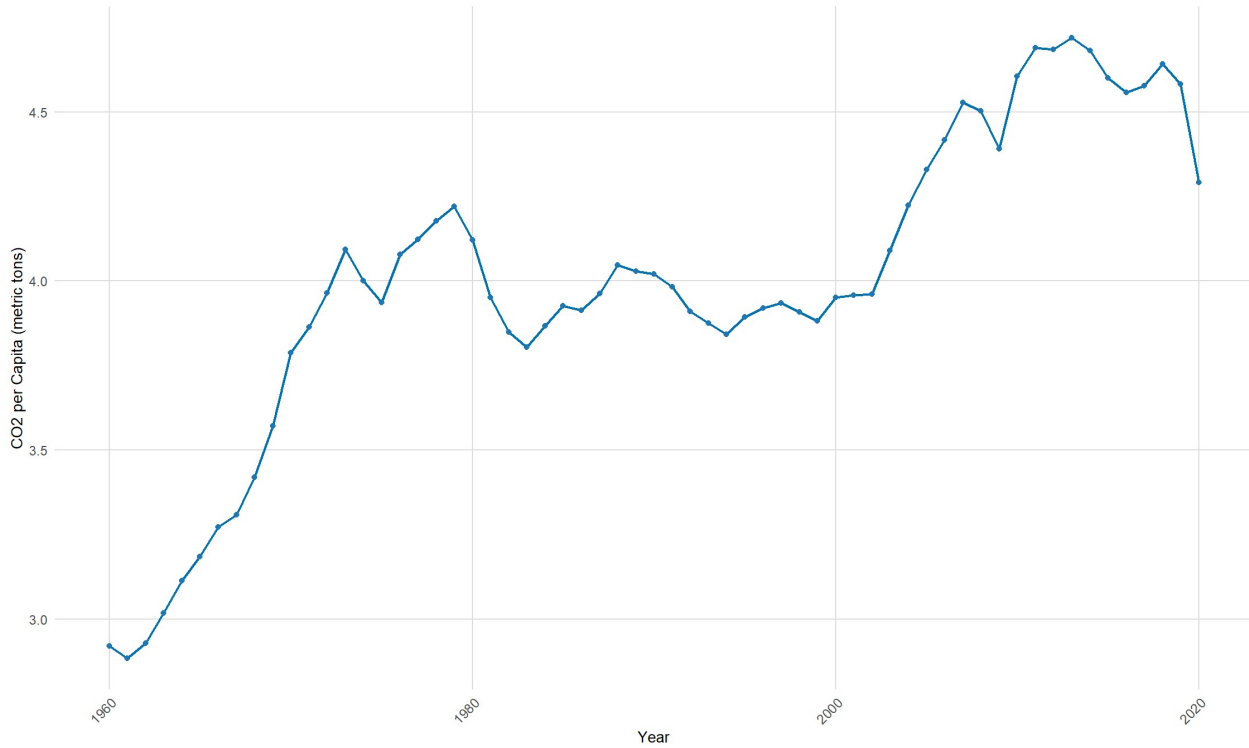


Figure 7. CO<sub>2</sub> emissions per capita (1960-2020)

Next, we examine the relationship between World CO<sub>2</sub> emissions per capita and the number of floods per region from 1960 to 2020. Figure 8 displays scatter plots illustrating this relationship. Notably, all regions exhibit a positive correlation, signifying that an increase in CO<sub>2</sub> emissions is associated with a corresponding rise in flood frequency. Moreover, we observe notably strong correlations (more than 0.70) in four regions specifically those

---

9. World CO<sub>2</sub> emissions speed up since 2000, <https://www.reuters.com/article/us-climate-emissions-idUSN2135818320070521>, Accessed: 2023-07-25

characterized as developing countries. These regions display a robust positive association between CO<sub>2</sub> emissions and flood occurrences. In contrast, Europe & Central Asia and North America demonstrate slightly lower correlations of 0.5 and 0.3, respectively, while still maintaining a positive relationship. These findings suggest that variations in CO<sub>2</sub> emissions play a role in influencing flood frequencies, with some regions displaying a stronger association than others.

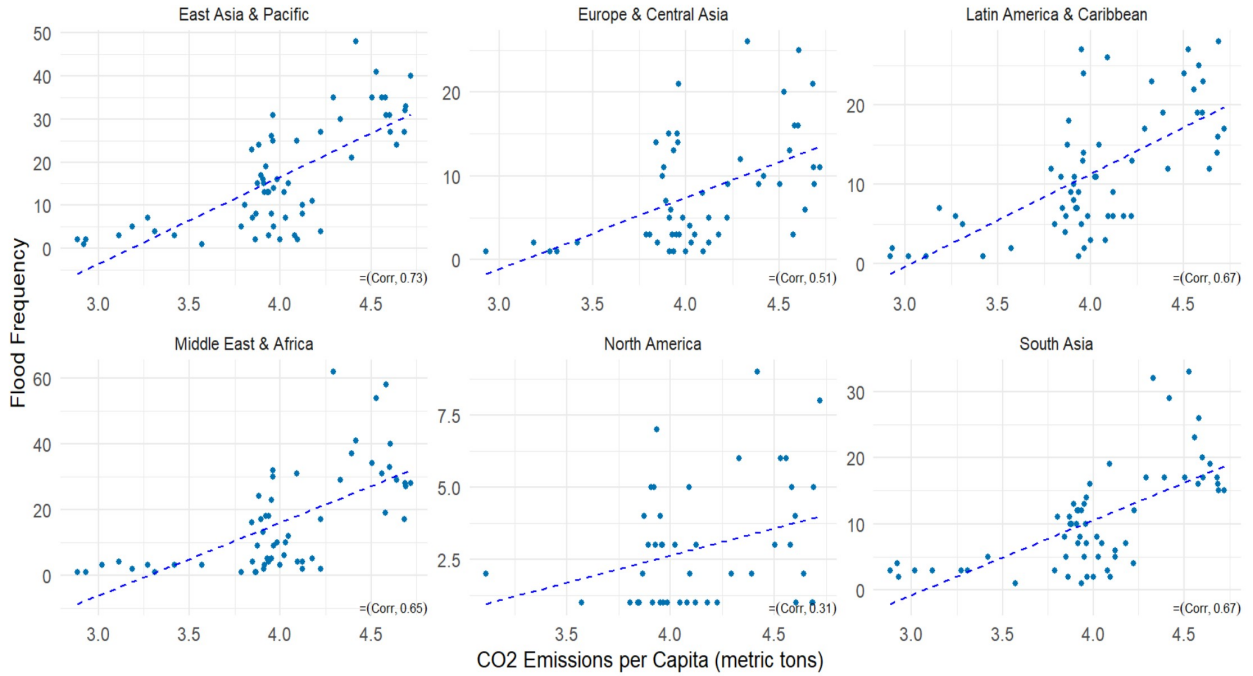


Figure 8. Correlation CO<sub>2</sub> emissions per capita and Number of Flood per region (1960-2020)

Subsequently, we conduct an analysis of the average number of deaths per event. It is crucial to underscore that our analysis employs the rescaled number of deaths, as determined by Equation 1. This rescaling method ensures the normalization of historical death tolls to the population in 2020, thus enabling a compatible and fair comparison of death tolls across different years.

Table 7 displays the average number of deaths per flood event in different regions. South Asia reports the highest Expected 415.5 deaths per event, indicating greater vulnerability to severe flood-related consequences. In contrast, North America exhibits the lowest Expected 19.9 deaths per event. The remaining regions show intermediate average death

tolls, with East Asia & Pacific at 133.3, Europe & Central Asia at 25.5, Latin America & Caribbean at 118.4, and Middle East & Africa at 68.1 deaths per event.

Table 7. Average Deaths per Flood each region

Regions	Average deaths
East Asia & Pacific	133.3
Europe & Central Asia	25.5
Latin America & Caribbean	118.4
Middle East & Africa	68.1
North America	19.9
South Asia	415.5

Figure 9 presents the evolution of the average number of deaths per flood event for all regions. Notably, the chart is displayed in log scale to address potential outliers resulting from extreme events, as certain regions might experience unusually high average values due to such occurrences. The observed trend across all regions showcases a notable decrease in the average death toll per flood event over time. This decline suggests the possibility of enhanced disaster risk management practices, contributing to a reduction in the human impact of floods in the studied regions.

Figure 10 displays the time series of GDP per capita for each region, sourced from the World Bank data, spanning from 1960 to 2020.

Figure 11<sup>10</sup> depicts the scatter plot and correlation analysis between GDP per capita and the average number of deaths per flood event across all regions. The chart reveals a negative correlation between GDP per capita and the average number of deaths per flood event in all regions. This negative correlation implies that as a country's wealth, represented by GDP per capita, increases, the average death toll per flood event decreases. This observation highlights the potential impact of economic prosperity on disaster management and infrastructure development, leading to enhanced disaster response and mitigation systems as the country's wealth increases.

---

10. The x-axis is capped at 800 for better readability, and South Asia has several large outliers, contributing to the relatively lower linear correlation in this region.

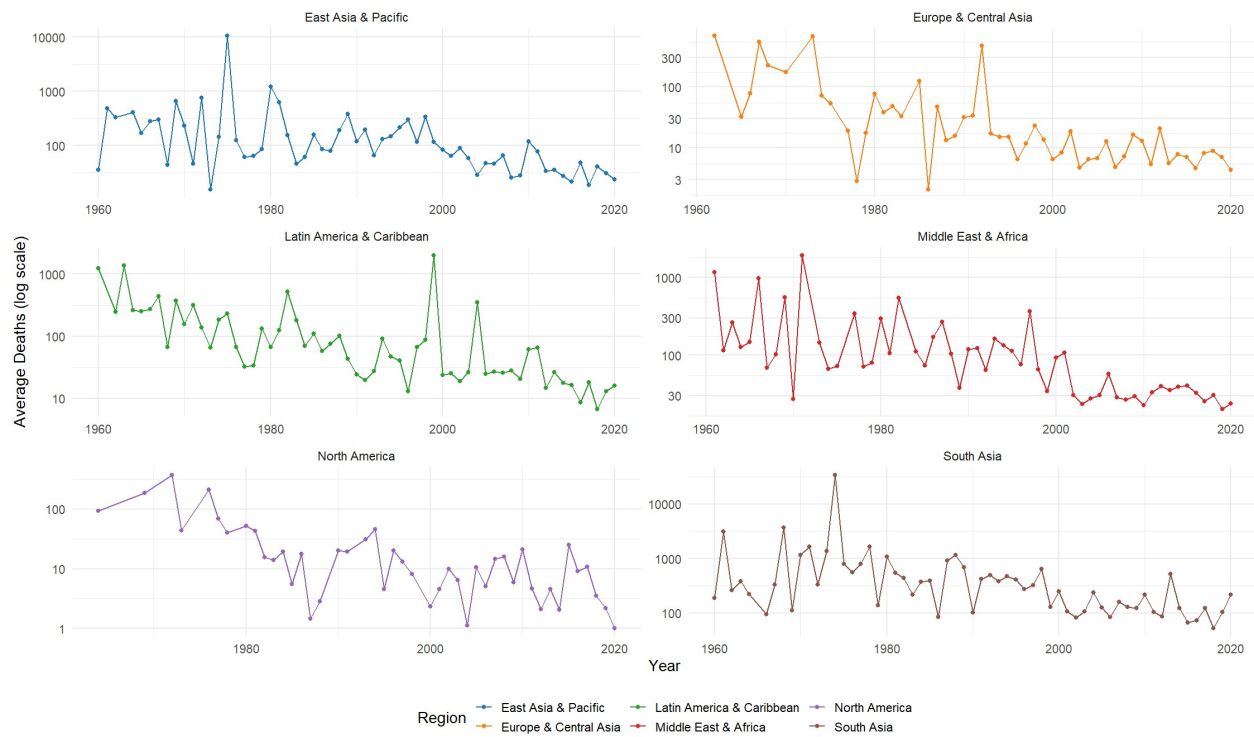


Figure 9. Average deaths per flood in log scale (1960-2020)

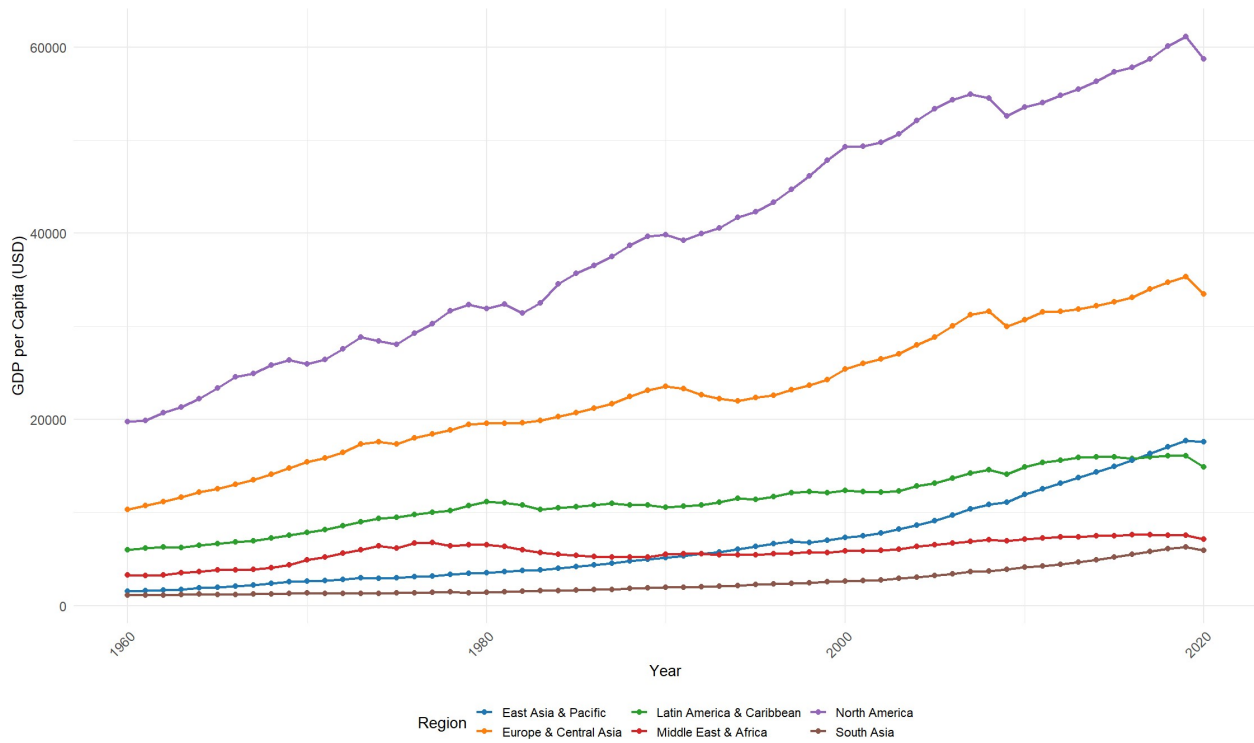


Figure 10. GDP per capita each region (1960-2020)

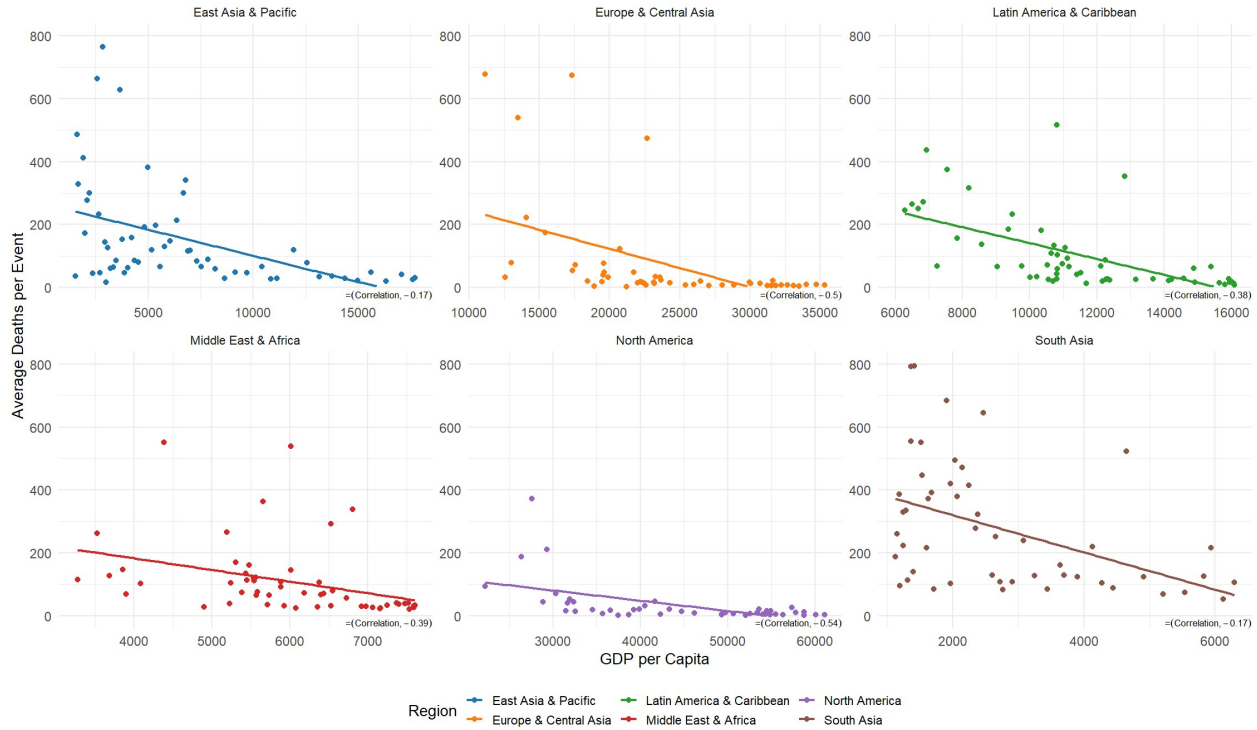


Figure 11. Correlation between GDP per capita and Average Deaths per flood (1960-2020)

Based on the previous charts, we observed an increasing trend in the frequency of flood occurrences over the last 20 years, while the average number of deaths per event has been decreasing. However, the net effect of these disasters remains uncertain. To gain a clearer understanding, we plotted the historical total deaths. Figure 12 presents the total death toll from floods for each 10-year period spanning from 1960 to 2020. The chart clearly indicates that during the past two decades, there has been a consistent decline in the total number of deaths caused by floods. This trend underscores a positive development in disaster management and preparedness efforts, resulting in reduced human losses in flood events over recent years.

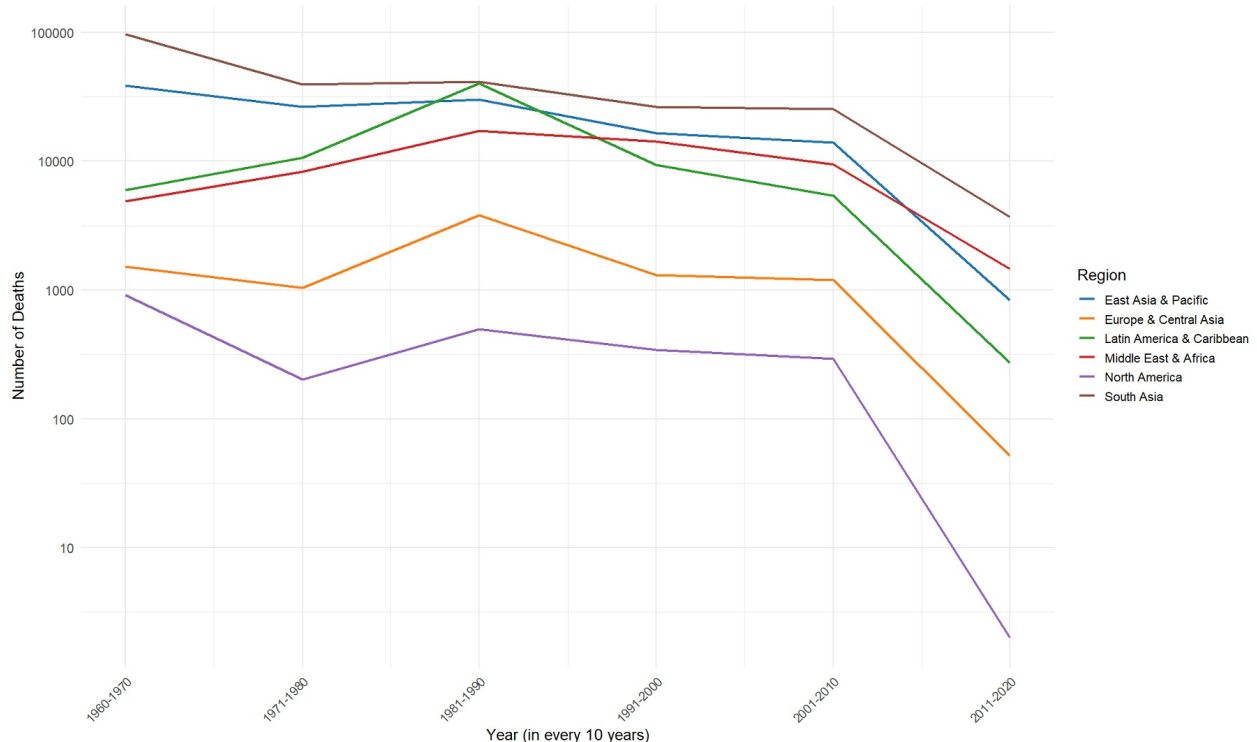


Figure 12. Total Deaths

## Exploratory Data Analysis of projections

In this subsection, we conduct an exploratory data analysis (EDA) of the IIASA-IPCC data.

Figure 13 illustrates the time series of CO<sub>2</sub> emissions per capita in metric tons for five selected scenarios, covering the period from 2020 to 2100 with intervals of 10 years. The analysis reveals trends in CO<sub>2</sub> emissions per capita across the scenarios:

*Decrease in SSP1-1.9, SSP1-2.6, and SSP2-4.5.* They exhibit a declining trend in CO<sub>2</sub> emissions per capita over time. This pattern suggests a decreasing reliance on carbon-intensive activities and a move towards more sustainable practices in these scenarios.

*Pointing out negative values for SSP1-1.9 and SSP1-2.6 after 2050.* Beyond the year 2050, both scenarios demonstrate a noteworthy feature of negative values in CO<sub>2</sub> emissions per capita. This peculiar behavior raises an interesting question and warrants further investigation. As a result, we limit our analysis up to the year 2050.

*Significant increase in SSP5-8.5.* The scenario stands out with a remarkable upsurge in CO<sub>2</sub> emissions per capita. The data indicates that this scenario experiences a substantial three-fold increase in emissions compared to the current levels. This substantial rise in emissions poses challenges in terms of climate change mitigation and necessitates careful consideration in policy planning.

*SSP3-7.0 shows limited change.* Contrary to the drastic changes observed in other scenarios, SSP3-7.0 demonstrates a comparatively stable pattern in CO<sub>2</sub> emissions per capita, indicating a relatively consistent path in this scenario.

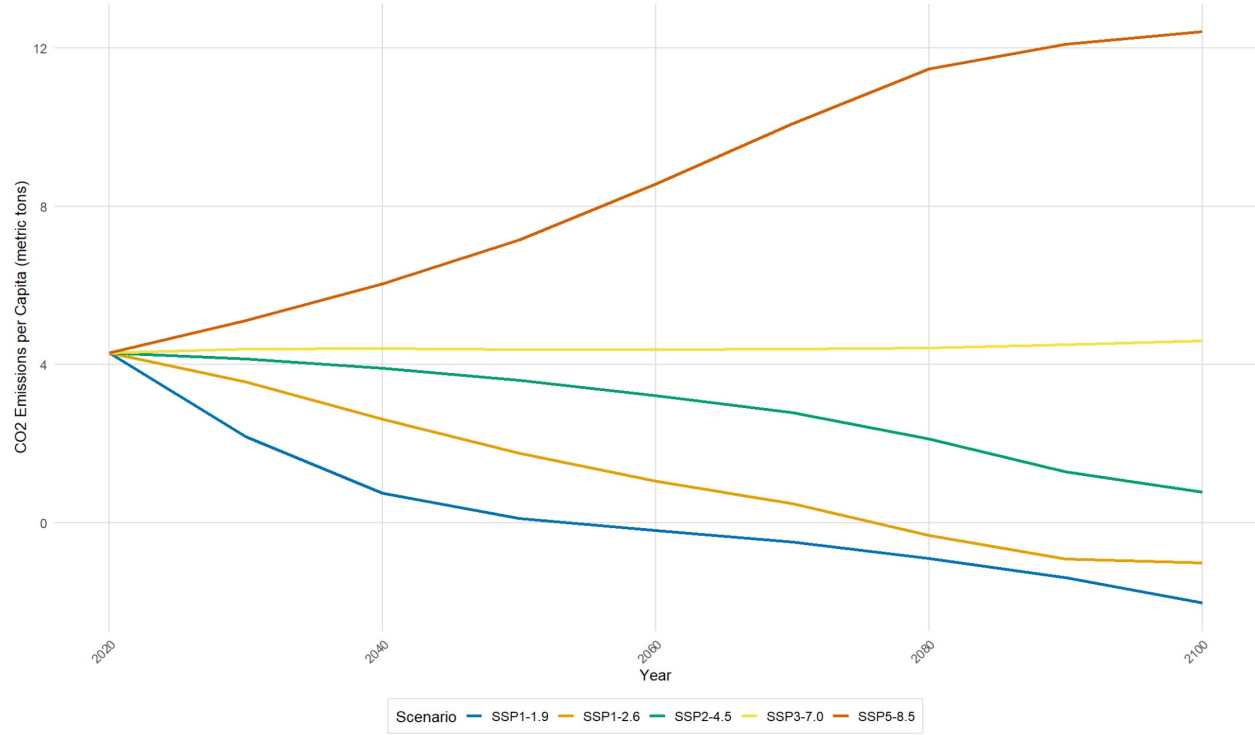


Figure 13. CO<sub>2</sub> Emissions per Capita Projections in the 5 Scenarios

Figure 14 presents a comprehensive time series analysis of GDP per capita for each region under the five selected scenarios (amounting to a total of six charts). The analysis spans from the year 2020 to 2100, with data intervals of 10 years. The examination of the data reveals significant disparities in GDP per capita trajectories across the scenarios and regions, providing crucial insights into economic growth prospects under varying socioeconomic conditions.

*SSP5-8.5: Highest GDP Growth Across All Regions.* An observation from the analysis is that the SSP5-8.5 consistently exhibits the highest GDP growth across all regions. This trend is particularly significant given the scenario's portrayal of a future world characterized by high population and rapid economic development, with little emphasis on environmental or climate concerns. The rationale behind this phenomenon can be attributed to several factors. Firstly, the SSP5-8.5 scenario assumes a continuation of current trends and practices, where economic growth takes precedence over environmental sustainability. Consequently, this scenario entails higher industrialization, increased energy consumption, and intensified resource extraction, leading to a surge in GDP growth. Additionally, the scenario foresees minimal efforts to mitigate climate change and restrains carbon emissions, which may strengthen economic productivity in the short term but may cause considerable risks in the long run.

*SSP1-1.9 and SSP1-2.6: Balancing Environmental Sustainability and Economic Growth in Low-Carbon Scenarios.* Surprisingly, despite being regarded as the most favorable in terms of CO<sub>2</sub> emissions reduction, rank as the second-best scenarios concerning GDP growth. These scenarios envision a future marked by rapid adoption of sustainable practices, ambitious climate policies, and significant investment in green technologies. The rationale behind their relatively lower GDP growth lies in the potential trade-offs between environmental protection and unrestricted economic expansion. While stringent climate measures may dampen certain economic activities that contribute to carbon emissions, they can also foster innovation and investment in cleaner technologies, creating new avenues for economic growth. Thus, although the GDP growth in SSP1-1.9 and SSP1-2.6 scenarios may not be the highest, the emphasis on sustainability and low-carbon development aligns with global climate goals and offers a more sustainable trajectory for the long term.

*SSP3: Lowest GDP Growth.* In contrast to the other scenarios, SSP3 emerges as the scenario with the lowest GDP growth across all regions. This scenario envisions a world where international cooperation and development ambitions are minimal, and each region primarily focuses on its own economic priorities. The lack of global collaboration may lead to increased trade barriers, restricted access to resources, and slower technological advancements, impeding overall economic growth. Additionally, the absence of concerted efforts to

mitigate climate change and promote sustainable practices may exacerbate environmental challenges, further impacting economic productivity.

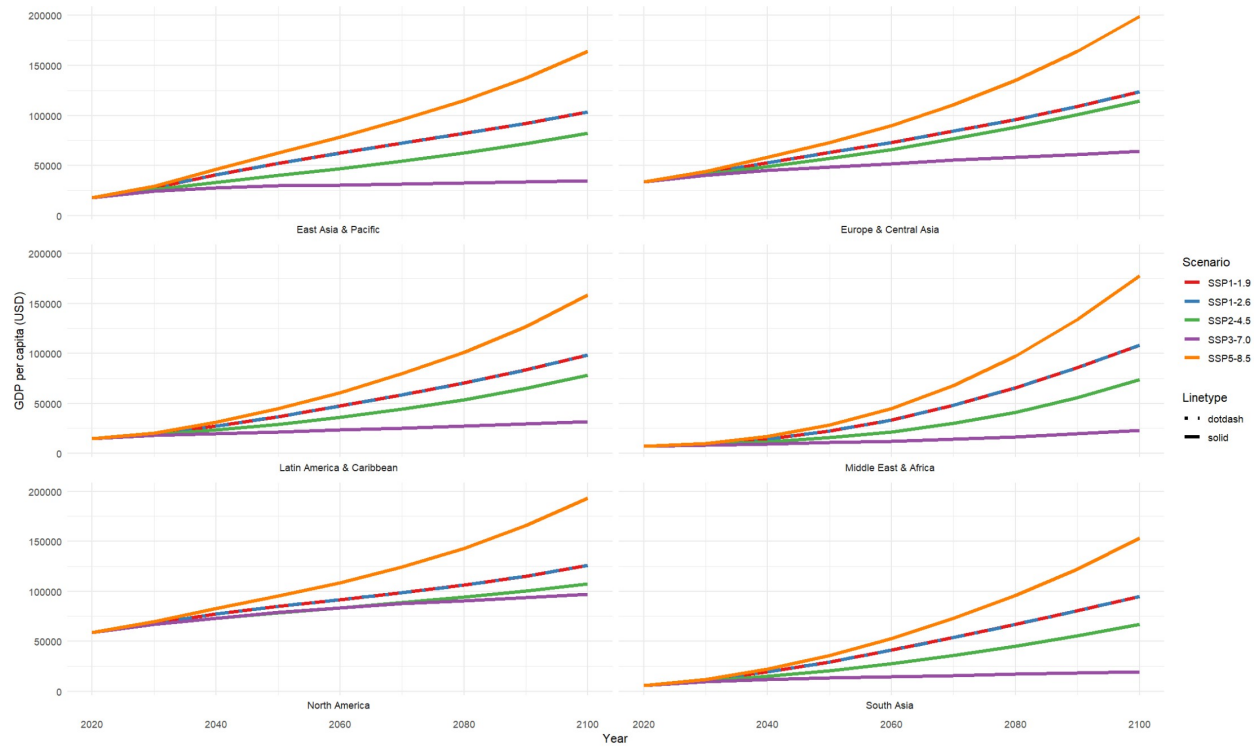


Figure 14. GDP per Capita Projections

### 3. Methodology and Modelling

In this thesis, we aim to introduce two comprehensive statistical models. The first model explains the evolution of the number of floods per year, denoted as  $N_t^{(r)}$ , at the regional level  $r$  during year  $t$ . The second model focuses on understanding the rescaled death toll per flood, denoted as  $\tilde{D}_t^{(r)}$ , for the regional level  $r$  in year  $t$ . By integrating these two models, we gain invaluable insights into the annual number of deaths attributable to floods, represented as  $S_t^{(r)}$ .

#### 3.1 Poisson distribution

We focus on studying a fundamental probability distribution widely used to analyse the occurrence of rare events - the Poisson distribution. Specifically, we employ the Poisson distribution to model the occurrence of floods in a given region over time. This modeling approach is based on the concept of a Poisson process, where the intensity parameter, denoted as  $\lambda_t^{(r)}$ , represent the expected number of occurrence for a given region  $r$  and year  $t$ .

The probability mass function of the Poisson distribution is given by:

$$P(N_t^{(r)} = k) = \frac{e^{-\lambda_t^{(r)}} (\lambda_t^{(r)})^k}{k!} \quad (5)$$

where

$P(N_t^{(r)} = k)$  is the probability of observing floods in the region during year  $t$ .

$\lambda_t^{(r)}$  is the intensity parameter, which represents the average rate of floods in the region during year  $t$ .

$k$  is the number of floods.

In the previous section, we have demonstrated that the frequency of floods displays non-stationary characteristics and a possible upward trend over time, which could be associated with the impact of climate change. To gain deeper insights into the underlying factors contributing to this observed pattern, we would like to explore the role of CO2 emissions per capita. In this study, we adopt log-transformed world CO2 emissions per capita as a covariate to model the frequency parameter.

Thus, our fundamental assumption is represented as follows:

$$\log(\lambda_t^{(r)}) = \lambda_0 + \sum_{i=1}^R \lambda_1^{(i)} \cdot D^{(i)} \cdot CO2_t + \epsilon_t^\lambda \quad (6)$$

where  $\log(\lambda_t^{(r)})$  denotes the log-transformed intensity parameter in the region  $r$  and year  $t$ .

$\lambda_0$  and  $\lambda_1^{(i)}$  are coefficients representing the intercept and the slope of the relationship between the logarithm of the frequency parameter of region  $i$  and the covariate  $CO2$ .

$R$  represents the number of regions.

$D^{(i)}$  represents a dummy variable, and is assumed a value of 1 when  $i$  corresponds to  $r$ ; otherwise, it assumes a value of 0

$CO2_t$  represents the log-transformed world CO2 emissions per capita in year  $t$ .

$\epsilon_t^\lambda$  represents the error term, capturing the variability and unexplained factors influencing the frequency parameter.

In this model, we aim to explain the relationship between CO2 emissions per capita and the frequency of floods, providing valuable insights into how changes in CO2 emissions per capita impact the occurrence of floods over time.

### 3.2 Generalized Pareto distribution

Flood-related death tolls often exhibit a heavy right tail, indicating that a few catastrophic floods contribute to a significant number of fatalities. This asymmetry demands the application of Extreme Value Theory (EVT) to understand extreme events accurately.

Figure 15 demonstrates a close fit to the exponential distribution for most data points from the international disaster database (EM-DAT) [12], which represent the number of deaths attributed to each separate flood event. However, at the upper end of the theoretical quantiles, a few data points deviate significantly from the theoretical line. This observation highlights the heavy-tailed nature of the data, where rare catastrophic floods lead to an unusually high number of deaths.

Extreme Value Theory (EVT) offers specialized tools to analyze heavy-tailed data, estimating tail parameters effectively. By leveraging EVT, we gain insights into the prob-

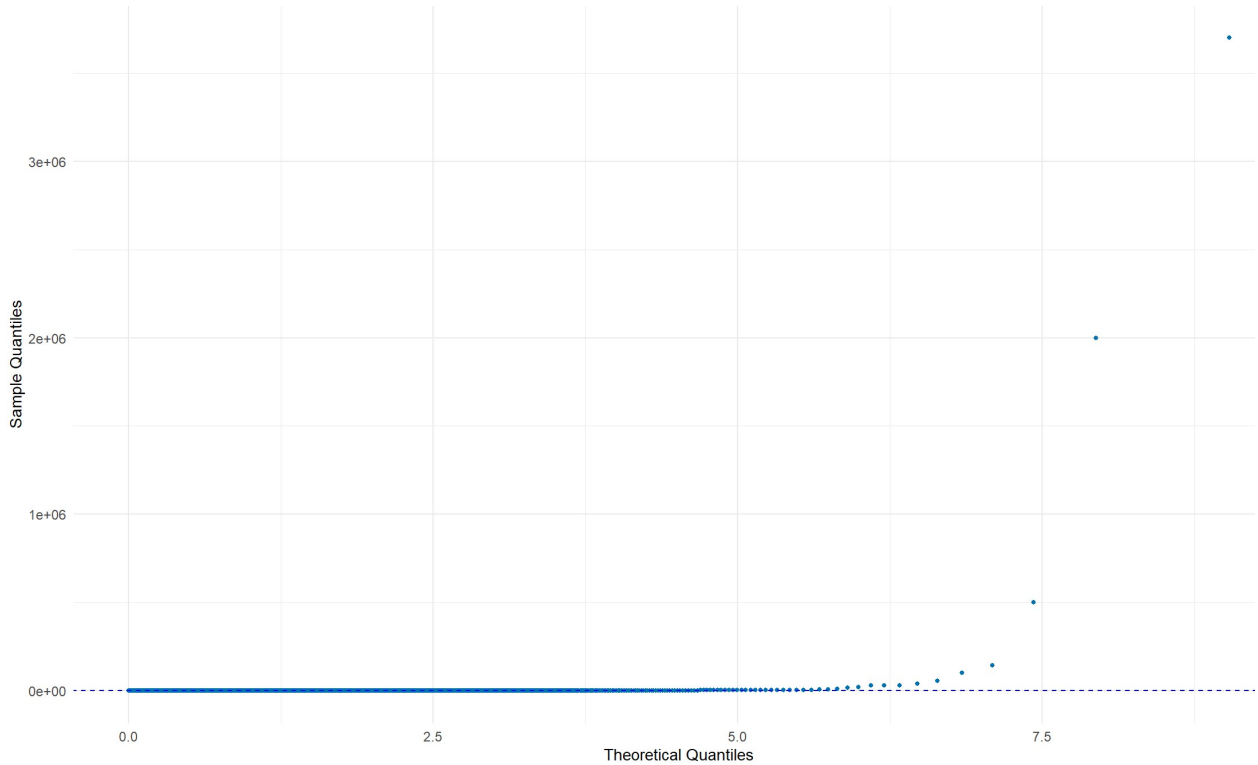


Figure 15. Exponential QQ plot of flood data

ability and severity of extreme flood events, improving risk assessment and management strategies. EVT typically considers two main approaches to analyse extreme events in data.

(1) *Block Maxima Approach:* The extreme values are identified within non-overlapping blocks of data, and the maximum value of each block is analyzed. The distribution of these block maxima is then analyzed to model extreme events. The Generalized Extreme Value (GEV) distribution is commonly used for this purpose. The GEV distribution represents the ultimate pattern of the rescaled maximum values from a series of independent and identically distributed (iid) variables obtained from most typical continuous distributions, as established by the Fisher-Tippett theorem.

(2) *Peaks-Over-Threshold (POT) Approach:* In contrast, this method focuses on the most severe events across the entire span of data collection. It necessitates setting a high threshold beyond which any points surpassing it are classified as extreme values. In the Peaks-Over-Threshold approach, the differences between data values and the threshold, known as exceedances or excesses, are pooled as a sample. This sample is assumed to be sourced from the generalized Pareto distribution (GPD).

The selection of the Peaks-Over-Threshold (POT) approach for our study stems from its aptness to address specific data characteristics. With the sparse occurrence of extreme flood events and occasional data gaps in certain regions, the POT method efficiently focuses on events surpassing a high threshold. This adaptive approach enables a thorough analysis of infrequent yet significant events. Moreover, the extensive time span of our dataset (1960-2020) aligns well with the POT method's capacity to capture key events across decades, facilitating trend identification.

When focusing on our database of extreme events of interest, the threshold  $\mu$  is inherently established at  $\mu = 0$ . This choice is motivated by the fact that our analysis is centered on events that exceed this baseline threshold. In practical terms, any event reaching or surpassing this threshold is categorized as one of the extreme events under consideration. This simplifies the calculation of the cumulative distribution function (CDF) of  $y \sim GPD(\xi, \beta)$  ( $\beta > 0$  and  $\xi > -1$ ), as the formula is adjusted accordingly to reflect this threshold  $\mu = 0$  configuration as follows. In essence, our chosen threshold aligns seamlessly with the nature of our dataset and the specific focus of our study.

$$G_{\xi_t^{(r)}, \beta_t^{(r)}}(y) = \begin{cases} 1 - \left(1 + \frac{\xi_t^{(r)}(y)}{\beta_t^{(r)}}\right)^{-1/\xi_t^{(r)}} & \text{if } \xi_t^{(r)} \neq 0 \\ 1 - \exp\left(-\frac{y}{\beta_t^{(r)}}\right) & \text{if } \xi_t^{(r)} = 0 \end{cases} \quad (7)$$

For  $y \geq 0$ , if  $\xi_t^{(r)} \geq 0$ , and  $y \in [0, -\frac{\beta_t^{(r)}}{\xi_t^{(r)}}]$ , if  $\xi_t^{(r)} < 0$

Where:  $y$  is the number of death per flood event.

$\beta_t^{(r)}$  is the scale parameter in the region  $r$  and year  $t$ . It determines the scale or size of the distribution and plays a role in stretching or compressing the distribution along the horizontal axis. A larger value of  $\beta$  results in a wider distribution, while a smaller value makes it narrower. In the context of extreme value analysis, the scale parameter is associated with the size or magnitude of extreme events.

$\xi_t^{(r)}$  is the shape parameter defining the tail of the distribution in the region  $r$  and year  $t$ . It characterizes the heaviness of the tail relative to the exponential distribution. The value of  $\xi$  indicates whether the tail of the distribution is thicker (positive) or lighter

(negative) than that of an exponential distribution. When  $\xi = 0$ , the distribution simplifies to the exponential distribution.

As highlighted earlier in the preceding section, it is evident that not only does the frequency of floods exhibit non-stationary characteristics, but the intensity of flood occurrences also displays a similar trait. One would expect that the number of fatalities per flood event should decrease over time, given the anticipated improvements in disaster risk management as nations progress economically. To attain a more profound comprehension of the underlying drivers contributing to this observed trend, a comprehensive investigation into the influence of GDP per capita becomes imperative. Accordingly, the present study embraces GDP per capita as a covariate within each specific region, with the intent of modeling the scale ( $\beta_t^{(r)}$ ) and shape ( $\xi_t^{(r)}$ ) parameters. The method of maximum likelihood is employed for the estimation of both parameters. Concerning the model estimation within the Generalized Pareto Distribution (GPD) framework, we reparametrize  $\beta_t^{(r)}$  by  $\nu_t^{(r)}$  where  $\nu_t^{(r)} = \log((1 + \xi_t^{(r)})\beta_t^{(r)})$ .

Consequently, our foundational hypothesis is formulated as follows:

$$\nu_t^{(r)} = \nu_0 + \sum_{i=1}^R \nu_1^{(i)} \cdot D^{(i)} \cdot GDP_t^{(i)} + \epsilon_t^\nu \quad (8)$$

$$\xi_t^{(r)} = \xi_0 + \sum_{i=1}^R \xi_1^{(i)} \cdot D^{(i)} \cdot GDP_t^{(i)} + \epsilon_t^\xi \quad (9)$$

where  $\nu_0$  and  $\nu_1^{(i)}$  are coefficients representing the intercept and the slope of the relationship between the scale parameter of the region  $i$  and the covariate  $GDP$ .

$\xi_0$  and  $\xi_1^{(i)}$  are coefficients representing the intercept and the slope of the relationship between the shape parameter of the region  $i$  and the covariate  $GDP$ .

$R$  represents the number of regions.

$D^{(i)}$  represents a dummy variable, and is assumed a value of 1 when  $i$  corresponds to  $r$ ; otherwise, it assumes a value of 0

$GDP_t^{(i)}$  represents the log-transformed real GDP per capita in the region  $i$  and year  $t$ .

$\epsilon_t^\nu$  and  $\epsilon_t^\xi$  represent the error term, capturing the variability and unexplained factors for scale and shape parameters respectively. Both are characterized as Gaussian noise with a mean of zero, signifying the absence of systematic bias in their influences on the parameters.

Then, we calculate the scale parameter  $\beta_t^{(r)}$  from  $\exp(\nu_t^{(r)})/(1+\xi_t^{(r)})$ .

Upon deriving the scale and shape parameters for each year across all regions, we employ these parameters to compute the anticipated value. This value signifies the projected number of deaths per flood incident. The expected value for the Generalized Pareto Distribution (GPD) can be expressed as:

$$E(\tilde{D}_t^{(r)}) = \frac{\beta_t^{(r)}}{1 - \xi_t^{(r)}} \quad (10)$$

The formula given by Equation 10 is valid only when  $\xi$  is less than 1. If  $\xi$  is 1 or greater, the result is infinite.

Returning to the section on Disaster-related data, we previously rescaled the historical number of deaths per flood incident spanning from 1960 to 2019 with the reference year of 2020. Having acquired the projected count of deaths per flood incident for the year  $2020 + h$ ,  $h$  represents a given time horizon or time interval used for forecasting or projecting into the future, our next step involves reverting to the original scale. This adjustment is made in accordance with the population projection specific to the given region, as outlined by the provided IPCC scenario. Ultimately, our determination of the predicted death count for the year  $2020 + h$  can describe as follows:

$$E[D_{2020+h}^{(r)}] = E[\tilde{D}_{2020+h}^{(r)}] \times \frac{P_{2020+h}^{(r)}}{P_{2020}^{(r)}} \quad (11)$$

Where  $P_{2020+h}^{(r)}$  denotes the projection of the population of region  $r$  in the year  $2020 + h$ ;  $h$  represents a temporal span employed for future projection purposes. In our projections, we operate under the assumption that the population growth in all countries within a specific region mirrors the population growth projected by the IIASA-IPCC for that particular region.

Lastly, the projection of the annual number of deaths is acquired as follows:

$$E[S_{2020+h}^{(r)}] = E[N_{2020+h}^{(r)}] \times E[D_{2020+h}^{(r)}] \quad (12)$$

Where  $E[S_{2020+h}^{(r)}]$  represents the expected annual number of deaths of region  $r$  in the year  $2020 + h$ .

$E[N_{2020+h}^{(r)}]$  represents the expected frequency of floods of region  $r$  in the year  $2020 + h$ . This value aligns with the intensity parameter ( $\lambda$ ) of the Poisson distribution.

$E[D_{2020+h}^{(r)}]$  represents the expected number of deaths per flood incident of region  $r$  in the year  $2020 + h$ .

### 3.3 Flow chart diagram

In this section, a comprehensive overview of the procedural steps is presented through the visual representation in Figure 16. The first function, denoted as Function 1, undertakes an analytical examination of historical data from 1960 to 2020, for the purpose of deriving coefficients to both the Poisson distribution and the Generalized Pareto Distribution (GPD). In the subsequent phase, denoted as Function 2, we apply the bootstrap method, a resampling technique that capitalizes on the variability of the dataset. By drawing repeated samples from the coefficients generated by Function 1, it facilitates the estimation of various annual parameters, bolstering the reliability of our forecasts in the face of data uncertainty. Within the scope of this thesis, we have carried out 200 simulations. Specifically, Function 2 projects the annual flood occurrence, the number of fatalities per flood event, and the annual cumulative death toll.

The detailed steps of Function 1 are based on combining three separate datasets as inputs, referring to the information highlighted in Section 2.1 about Disaster-related Data and the data discussed in Section 2.3 regarding Historical Covariates. The aggregation of input data encompasses: (1) The EM-DAT dataset post normalization with respect to a reference base year, 2020. (2) The World CO2 emissions per capita, sourced from the World Bank Open Data. (3) GDP PPP per capita, also sourced from the World Bank Open Data.

Subsequently, the EM-DAT dataset and the World CO2 emissions per capita are employed as inputs for the Poisson fit, expressed as Equation 6, facilitating the derivation

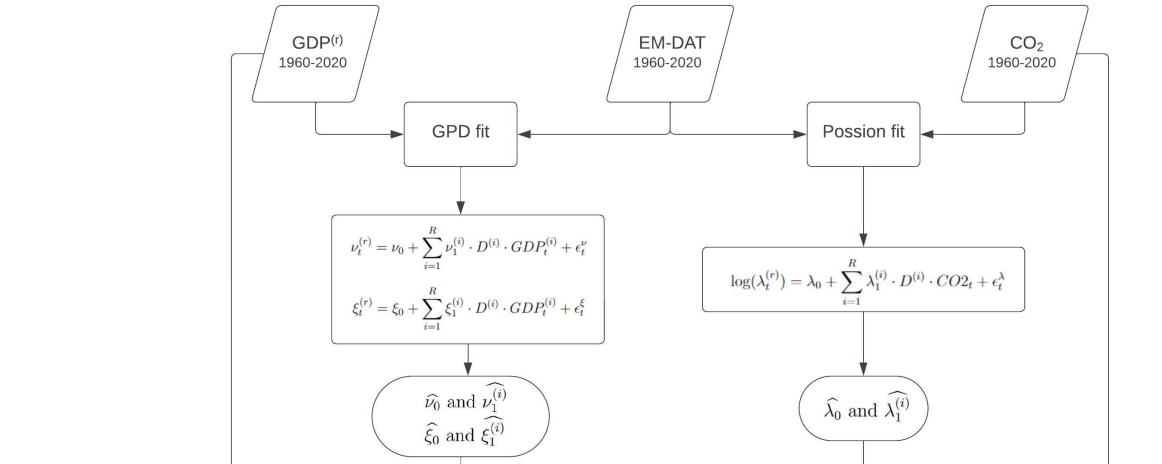
of estimated coefficients ( $\widehat{\lambda}_0$  and  $\widehat{\lambda}_1^{(i)}$ ) for each region encompassed by the model. A similar method is employed to determine the estimated coefficients of the GPD model. In this regard, the EM-DAT dataset is coupled with the GDP PPP per capita and employed as inputs for GPD fits, denoted as Equations 8 and 9. This process results in the acquisition of the estimated coefficients ( $\widehat{\nu}_0$ ,  $\widehat{\nu}_1^{(i)}$ ,  $\widehat{\xi}_0$ , and  $\widehat{\xi}_1^{(i)}$ ).

Function 2 applies the estimated coefficients derived from Function 1, along with their standard errors from the model, to conduct simulations and obtain the simulated estimates of the parameters. Then, the Poisson model (6) incorporates the World CO<sub>2</sub> emissions per capita to compute the expected number of floods ( $\widehat{\lambda}_t^{(r)}$ ) for each region annually (from 1960 to 2020). Subsequently, the GPD model (8 and 9) is employed with the GDP PPP per capita data to establish the Generalized Pareto Distribution of the number of deaths per flood event. Subsequently, these updated Poisson and GPD distributions are used for simulating both the historical frequency of flood events and the death toll for each event (1960-2020). This process results in the creation of a simulated EM-DAT dataset, referred to as the New EM-DAT.

Afterward, the procedures outlined in Function 1 are reiterated, and projected CO<sub>2</sub> emissions per capita and GDP PPP per capita from 2030 to 2050, sourced from IIASA-IPCC, are used for each scenario. We then compute the projections of the estimated parameters ( $\widehat{\lambda}_t^{(r)}$ ,  $\widehat{\nu}_t^{(r)}$ , and  $\widehat{\xi}_t^{(r)}$ ) within both the Poisson distribution and the GPD.

With the bootstrap technique, we repeat all steps in Function 2 for a total of 200 iterations to enhance the robustness of the outcomes. Finally, leveraging the derived information, we forecast the expected number of floods for each region in the 2030-2050 time frame, represented by the intensity parameter ( $\widehat{\lambda}_t^{(r)}$ ). Additionally, we predict the number of deaths per flood event for each region in the same timeframe by using the expected values of the GPD, referencing Equation 10 with respect to  $\widehat{\nu}_t^{(r)}$ , and  $\widehat{\xi}_t^{(r)}$ . To compute the annual deaths for each region, the number of deaths per flood event must be adjusted from the 2020 population assumption back to its initial scale (projected populations) using Equation 11. This recalibration accounts for their prior rescaling to the reference year 2020, as explained in Equation 1 within Section 2.1 Disaster-related data. Subsequently, the calculation of annual deaths for each region can be conducted using Equation 12.

### Function 1



### Function 2

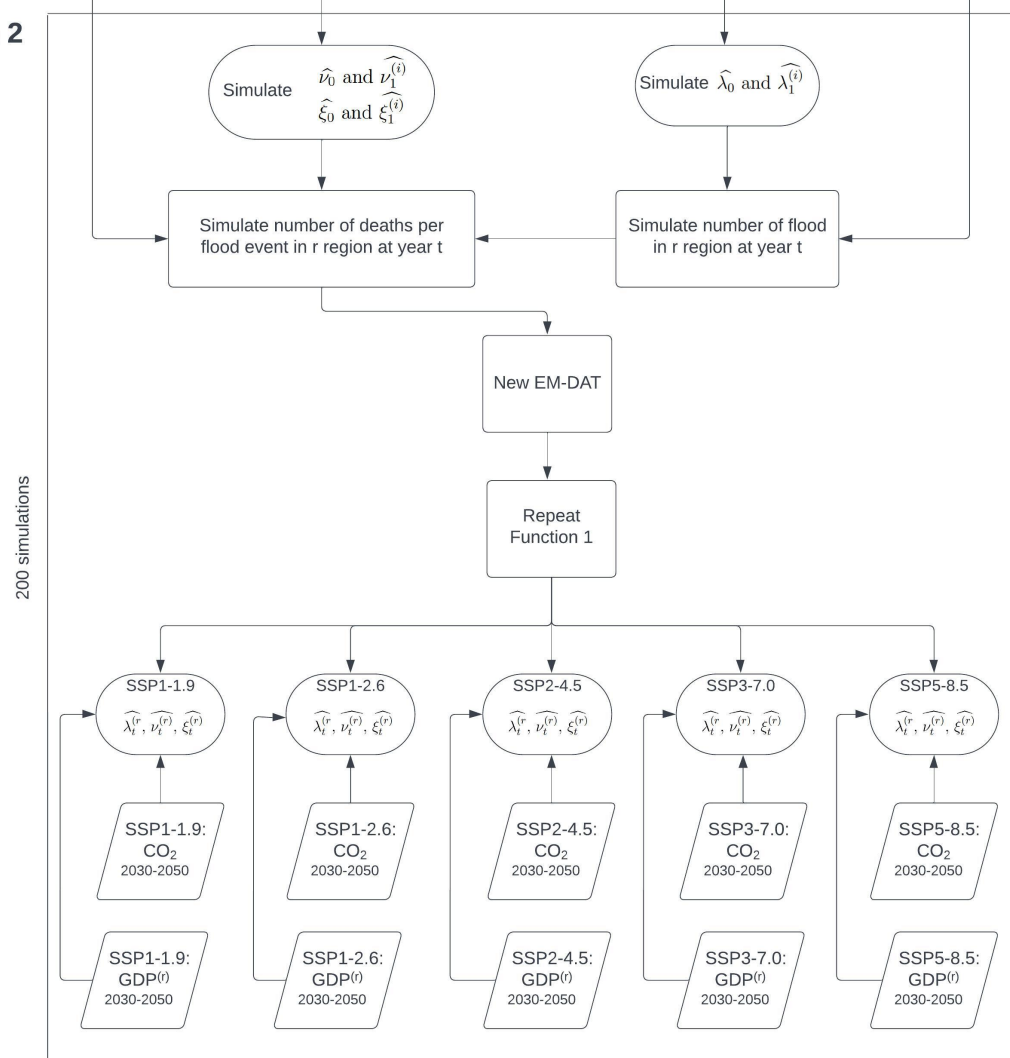


Figure 16. Flowchart Illustrating Parameter Estimation for Poisson Distribution and Generalized Pareto Distribution (GPD)

## 4. Results

### 4.1 Frequency

#### Estimation Results

In the presented Poisson-Frequency model, both the dependent (intensity parameter) and independent ( $CO_2$ ) variables undergo a log transformation, as indicated in Equation 6. Such a transformation results in what is typically referred to as a log-log model. In this context, the coefficients, represented as  $\beta$ , denote the elasticity of the dependent variable  $y$  with respect to the independent variable  $x$ . Essentially, elasticity gauges how a percentage change in one variable, in this case  $x$ , influences a percentage change in  $y$ . To illustrate, when we interpret the coefficient  $\beta$ , we understand it as the expected percent change in  $y$  for every one percent change in  $x$ . Thus, if  $\beta$  were 5, a 1% increase in  $x$  would lead to an approximate 5% increase in  $y$ . Likewise, a  $\beta$  of -5 would suggest that a 1% increase in  $x$  corresponds to a 5% decrease in  $y$ .

Table 8 shows that the relationship between flood frequency and aggregate  $CO_2$  emissions is predominantly positive and statistically significant at the 99.9% confidence level across regions. Additionally, the adjusted R-squared for this model is 58.3% further attesting to the model's ability to explain the variance. Each region-specific coefficient explains the percentage change in flood frequency associated with a 1% increase in  $CO_2$  emissions for that region. For instance, a coefficient of 6.2890 for East Asia & Pacific suggests that a 1% increase in  $CO_2$  emissions in that region corresponds to a 6.2890% rise in flood frequency, holding other factors constant. The table also shows distinct variations in the sensitivity of flood frequency to  $CO_2$  emissions across regions. The coefficient for *East Asia & Pacific* holds the highest magnitude at 6.2890, indicating this region's heightened sensitivity to changes in  $CO_2$  emissions in relation to flood frequency. In contrast, *North America* displays a comparatively lowered sensitivity with a coefficient of 4.8799.

Figure 17 presents the historical annual counts of flood occurrences for each region from 1960 to 2020, compared with the expected frequencies predicted by the model. Meanwhile, Figure 18 displays the same data in a scatter plot, where the y-axis shows the actual

	Estimate	Standard Error
Intercept	-6.0931***	0.2626
$\log(CO_2) \times D_{\text{East Asia \& Pacific}}$	6.2890***	0.1823
$\log(CO_2) \times D_{\text{Europe \& Central Asia}}$	5.6877***	0.1847
$\log(CO_2) \times D_{\text{Latin America \& Caribbean}}$	6.0219***	0.1832
$\log(CO_2) \times D_{\text{Middle East \& Africa}}$	6.2379***	0.1825
$\log(CO_2) \times D_{\text{North America}}$	4.8799***	0.1922
$\log(CO_2) \times D_{\text{South Asia}}$	5.9702***	0.1834
Adjusted R-squared	0.583	
Observations	366	

Table 8. Parameter estimation ( $\lambda$ ) of the Poisson-Frequency model: \*\*\* p<0.001, \*\* p<0.01, \* p<0.05

flood counts and the x-axis represents the expected counts from the model. From the analysis of both figures, it is evident that our model tends to overestimate at the beginning of the time series or during periods of low frequency. Subsequently, there is an underestimation around the midpoint of the time series. Nevertheless, the model's accuracy improves notably in recent years for specific regions such as East Asia Pacific, Latin America, and South Asia. It is crucial to acknowledge that the model's performance is subpar for the North America region, potentially attributed to a limited sample size.

## Projections

As we observed from Figure 13, the IIASA-IPCC projection suggests the following trends in carbon emissions across different scenarios. In SSP1-1.9 and SSP1-2.6, there is a decline in CO<sub>2</sub> emissions. Notably, SSP1-1.9 anticipates nearing net-zero carbon emissions in the year 2050. Conversely, SSP3-7.0 exhibits relatively stable emissions levels, with minimal fluctuations. In SSP5-8.5, carbon emissions experience a significant surge, showing an estimated rise of almost 200%.

In Figure 19, we present the projected trajectory of flood occurrences, starting from the baseline period (2011-2020) and extending to 2050. For a comprehensive breakdown of these projections, one may refer to Tables A1 through A5 located in Appendix A.

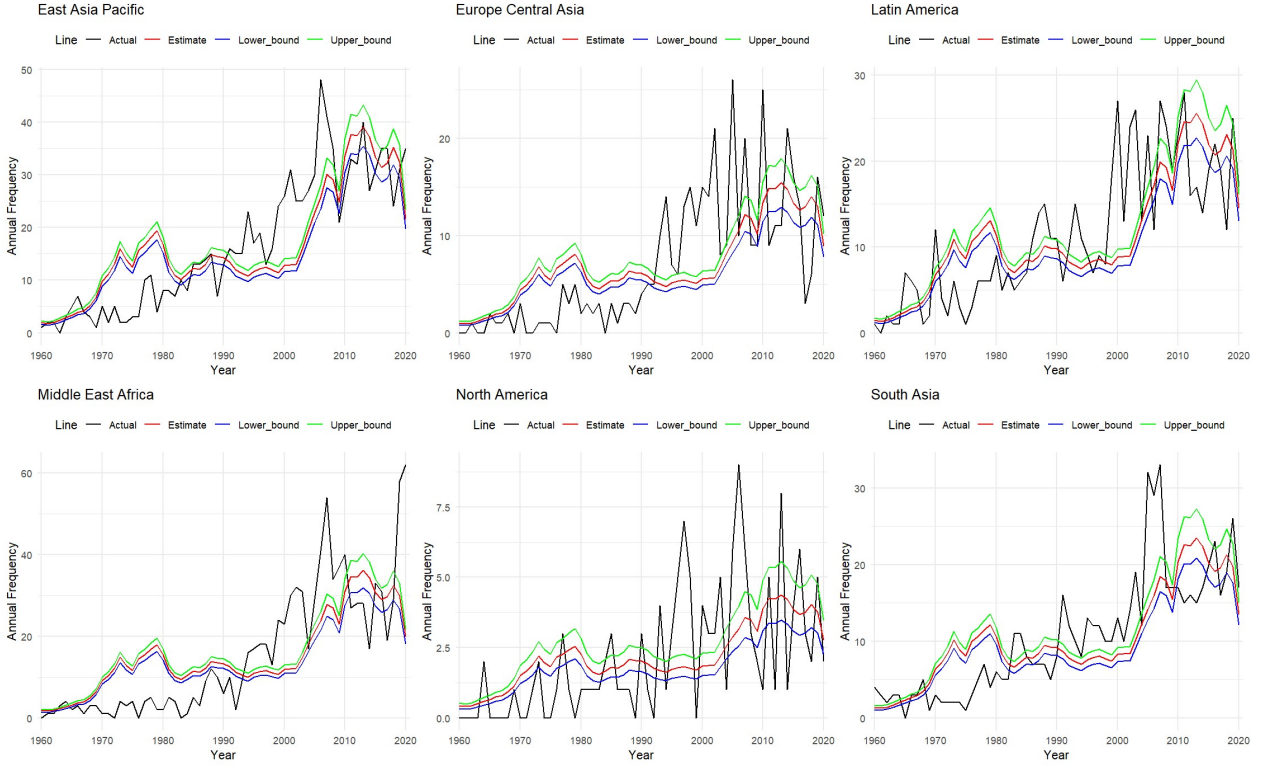


Figure 17. Frequency of Flood from 1960 to 2020. The black line represents the actual data, the red line denotes the expected frequency from the model, and the blue and green lines represent the lower and upper bounds of the 95% confidence interval, respectively.

The simulation results for various SSPs offer insights into the projected trends in flood events across different time horizons. In the context of the SSP1-1.9 scenario, an aggressive reduction in flood incidents is foreseen. From an initial average of 124.9 flood events annually during 2011-2020, the model anticipates almost no floods across all regions by 2050. In the case of SSP1-2.6, a consistent downward trajectory in flood events is evident. The expected annual frequency drops notably to 26.5 by 2030 and continues to diminish, nearly reaching an inconsequential 0.4 occurrences by 2050. Similarly, the SSP2-4.5 scenario demonstrates a more moderate decline. Starting from the baseline of 124.9 flood events between 2011-2020, annual counts progressively decrease to 66.2 by 2030 and further to 28.5 by 2050. Conversely, the SSP3-7.0 scenario showcases a slight reduction in flood occurrences over the decades. Notably, the SSP5-8.5 scenario stands apart by predicting a substantial upsurge in flood events. Contrary to the earlier scenarios, the number of floods escalates significantly from 124.9 events in 2011-2020 to a striking 1793.6 events per annum by 2050.

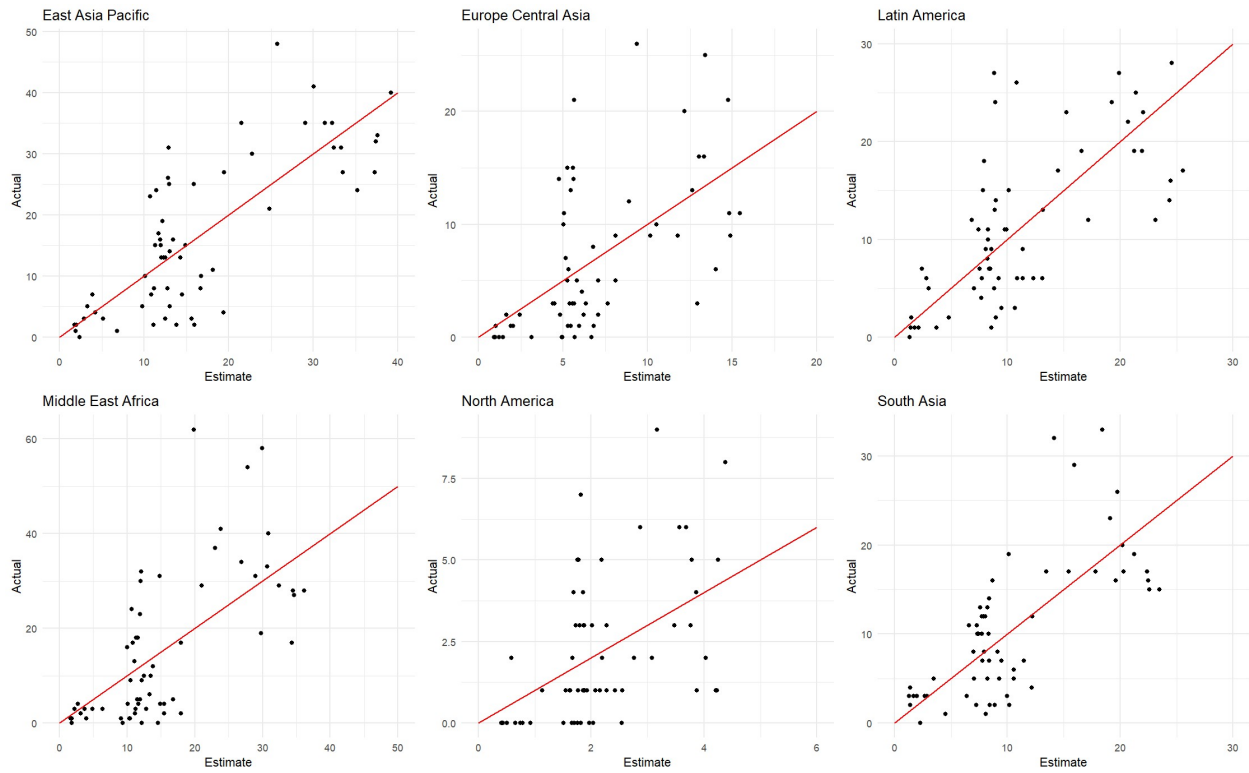


Figure 18. Scatter Plot Comparing Actual Flood Frequency with Model-Estimated Expected Frequency

In summary, while SS1-1.9 through SSP3-7.0 demonstrate diverse extents of decline in flood events, SSP5-8.5 presents a serious outlook, indicating that this scenario may result in a dramatic surge in flood frequency.

#### 4.2 Severity

### Estimation Results

In the analysis of the GPD-Severity model, we present the estimated outcomes for the parameters  $\nu$  and  $\xi$ , as detailed in Table 9 and Table 10, respectively. A clear observation from the results indicates that both parameters,  $\nu$  and  $\xi$ , exhibit significant negative associations with  $\log(\text{GDP})$ . Notably, these relationships are statistically significant at the 99.9% confidence level. This underscores the potential influence of a region's economic stature, as represented by GDP, on the severity, in terms of the death toll per event.

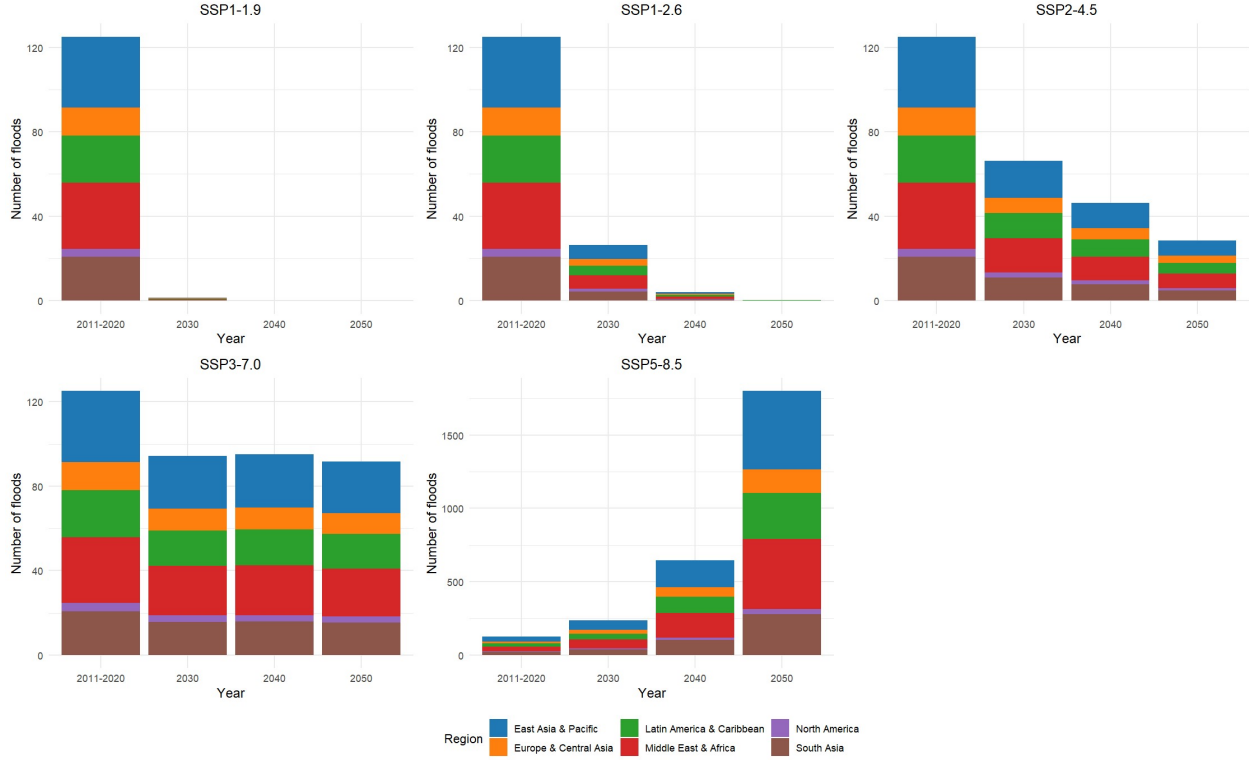


Figure 19. Projections of Frequency of Flood (all scenarios)

From Table 9, it is apparent that the adjusted R-squared value is 0.151. This implies that the model accounts for approximately 15.1% of the variance in the scale parameter of flood severity. Further scrutiny reveals that the interaction effects of log(GDP) with East Asia & Pacific and South Asia regions are relatively less pronounced than in other regions. This suggests that for a similar percentage growth in GDP, the reduction in loss severity in these two regions is not as pronounced as in other areas.

As shown in Table 10, the adjusted R-squared stands at 0.0474, suggesting that the model explains roughly 4.7% of the variability in the shape parameter associated with flood severity. The relative sensitivities across the different regions appear to be largely consistent.

Figure 20 depicts the historical average death count per event for each region between 1960 and 2020, compared with the expected death count per event as estimated by the GPD model. It is important to highlight that during the tail index estimation for the regions of East Asia & Pacific and South Asia, there were instances where the value of  $\xi$  was larger than 1, mainly in the earlier parts of the time series. Given that the expected value of

Scale Parameter ( $\nu$ )	Estimate	Standard Error
Intercept	14.3293***	1.3027
$D_{\text{Europe \& Central Asia}}$	19.9536***	5.6664
$D_{\text{Latin America \& Caribbean}}$	22.1610***	4.2349
$D_{\text{Middle East \& Africa}}$	18.5447***	4.6384
$D_{\text{North America}}$	23.4585***	7.1095
$D_{\text{South Asia}}$	2.0077	2.1049
$\log(\text{GDP}) \times D_{\text{East Asia \& Pacific}}$	-1.1543***	0.1426
$\log(\text{GDP}) \times D_{\text{Europe \& Central Asia}}$	-3.1273***	0.5394
$\log(\text{GDP}) \times D_{\text{Latin America \& Caribbean}}$	-3.4946***	0.4262
$\log(\text{GDP}) \times D_{\text{Middle East \& Africa}}$	-3.3304***	0.5061
$\log(\text{GDP}) \times D_{\text{North America}}$	-3.2737***	0.6480
$\log(\text{GDP}) \times D_{\text{South Asia}}$	-1.4190***	0.2043
Adjusted R-squared	0.151	
Observations	3,818	

Table 9. Parameter estimation ( $\nu$ ) of the GPD-Severity model: \*\*\* p<0.001, \*\* p<0.01, \* p<0.05

Shape Parameter ( $\xi$ )	Estimate	Standard Error
Intercept	3.13478***	0.32793
$\log(\text{GDP}) \times D_{\text{East Asia \& Pacific}}$	-0.27044***	0.03599
$\log(\text{GDP}) \times D_{\text{Europe \& Central Asia}}$	-0.25728***	0.03234
$\log(\text{GDP}) \times D_{\text{Latin America \& Caribbean}}$	-0.26459***	0.03480
$\log(\text{GDP}) \times D_{\text{Middle East \& Africa}}$	-0.29545***	0.03748
$\log(\text{GDP}) \times D_{\text{North America}}$	-0.28292***	0.03086
$\log(\text{GDP}) \times D_{\text{South Asia}}$	-0.29502***	0.04057
Adjusted R-squared	0.0474	
Observations	3,818	

Table 10. Parameter estimation ( $\xi$ ) of the GPD-Severity model: \*\*\* p<0.001, \*\* p<0.01, \* p<0.05

the GPD becomes infinite in these cases, we marked these instances as *n/a*. Our model's subsequent calculations only considered instances where  $\xi$  remained below 1. Nevertheless, for these regions, instances where  $\xi$  values neared 1 can account for the prominent upper bounds observed in Figure 20.

Similarly, Figure 21 presents this dataset in a scatter plot format. In this plot, the y-axis represents the actual average death count per event, while the x-axis illustrates the model's expected death count per event. The visualization reveals a noticeable trend in

the East Asia & Pacific, South Asia, and Latin America regions, where the model appears inclined toward overestimating the severity of losses. This is evident from the predominance of data points leaning towards the right side of the diagonal line.

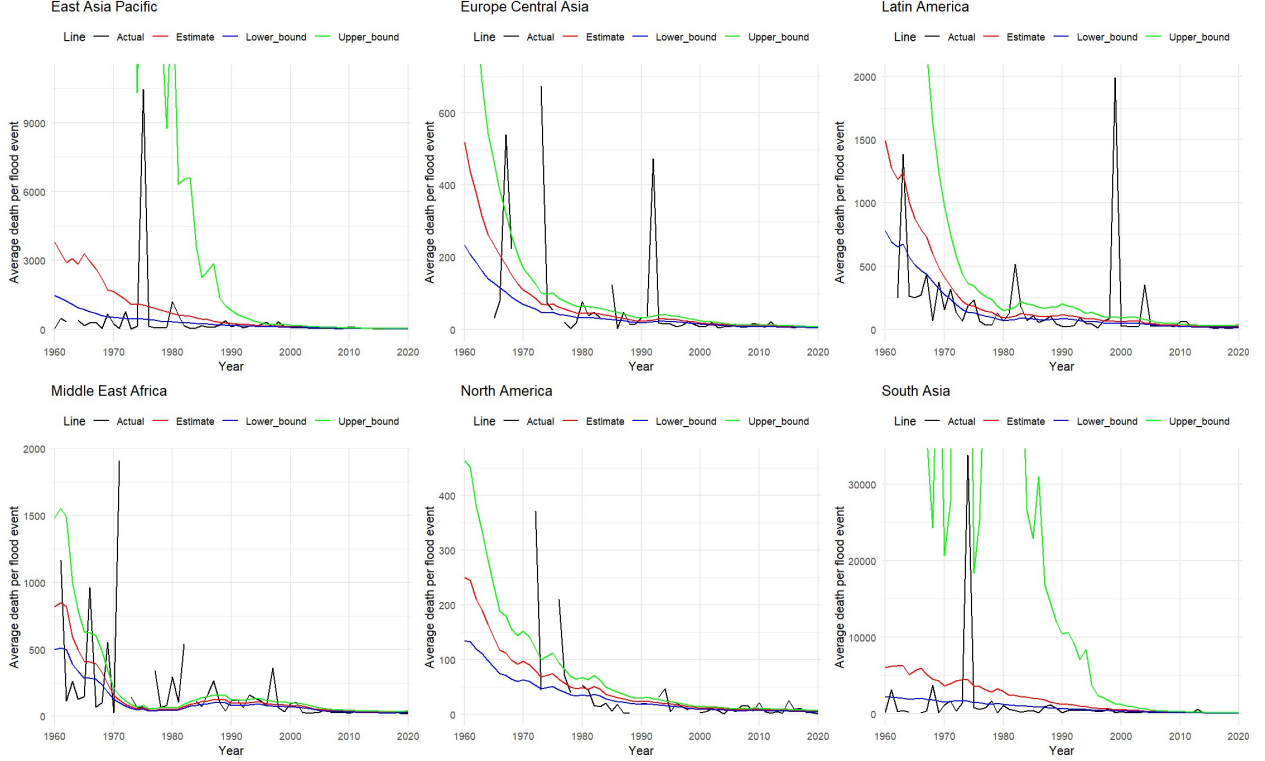


Figure 20. Average death per flood event from 1960 to 2020. The black line represents the actual data, the red line denotes the expected death per flood event from the model, and the blue and green lines represent the lower and upper bounds of the 95% confidence interval, respectively.

## Projections

This section presents the outcomes of the severity projections related to the average number of deaths per flood event. Initially, we employ the GDP PPP projections as provided by IIASA-IPCC to the model. It is important to note that the values generated by the model are based on the population figures as of the year 2020. Consequently, to align the predictions with projected population changes, we incorporate the population projections outlined in the IPCC scenarios into Equation 11. This enables the computation of a projected average death count per event, based on the forecasted population.

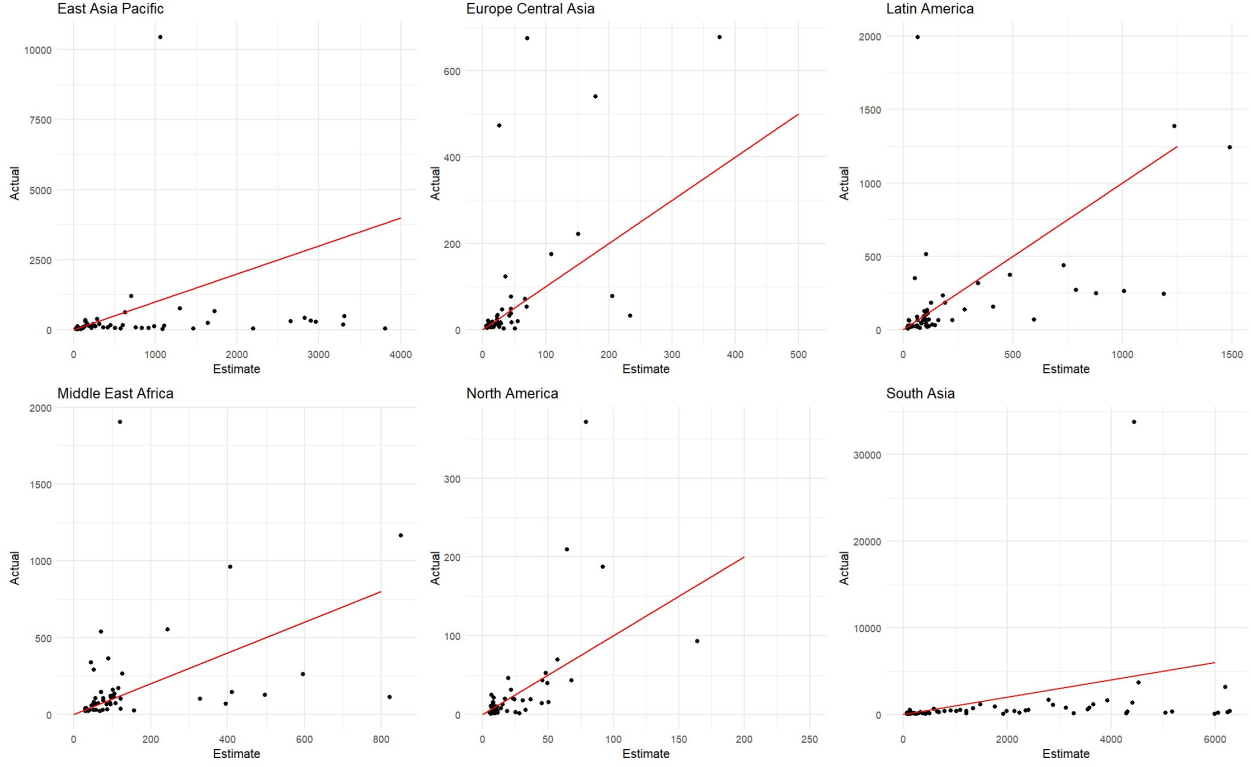


Figure 21. Scatter Plot Comparing Actual Severity per flood event with Model-Estimated Severity

The results correspond with the observations in Figure 14, which visualizes the most substantial GDP growth in SSP5-8.5, followed by SSP1, including SSP1-1.9 and SSP1-2.6 (both are equivalent). In contrast, the GDP growth in SSP3 is relatively modest. Figure 22 illustrates the projections of loss severity per event from the GPD model and shows that the SSP5-8.5 Scenario experiences the most significant reduction in the severity of losses per event. For instance, the anticipated number of deaths per event in South Asia averaged at 99.2 during the 2011 - 2020 period, sharply decreasing to 5.0 by 2050. This decline in loss severity is most pronounced in the SSP5-8.5 Scenario, while the smallest reduction is observed in the SSP3-7.0 scenario. To obtain a detailed analysis of these forecasts, one may refer to Tables B1 through B4 found in Appendix B.

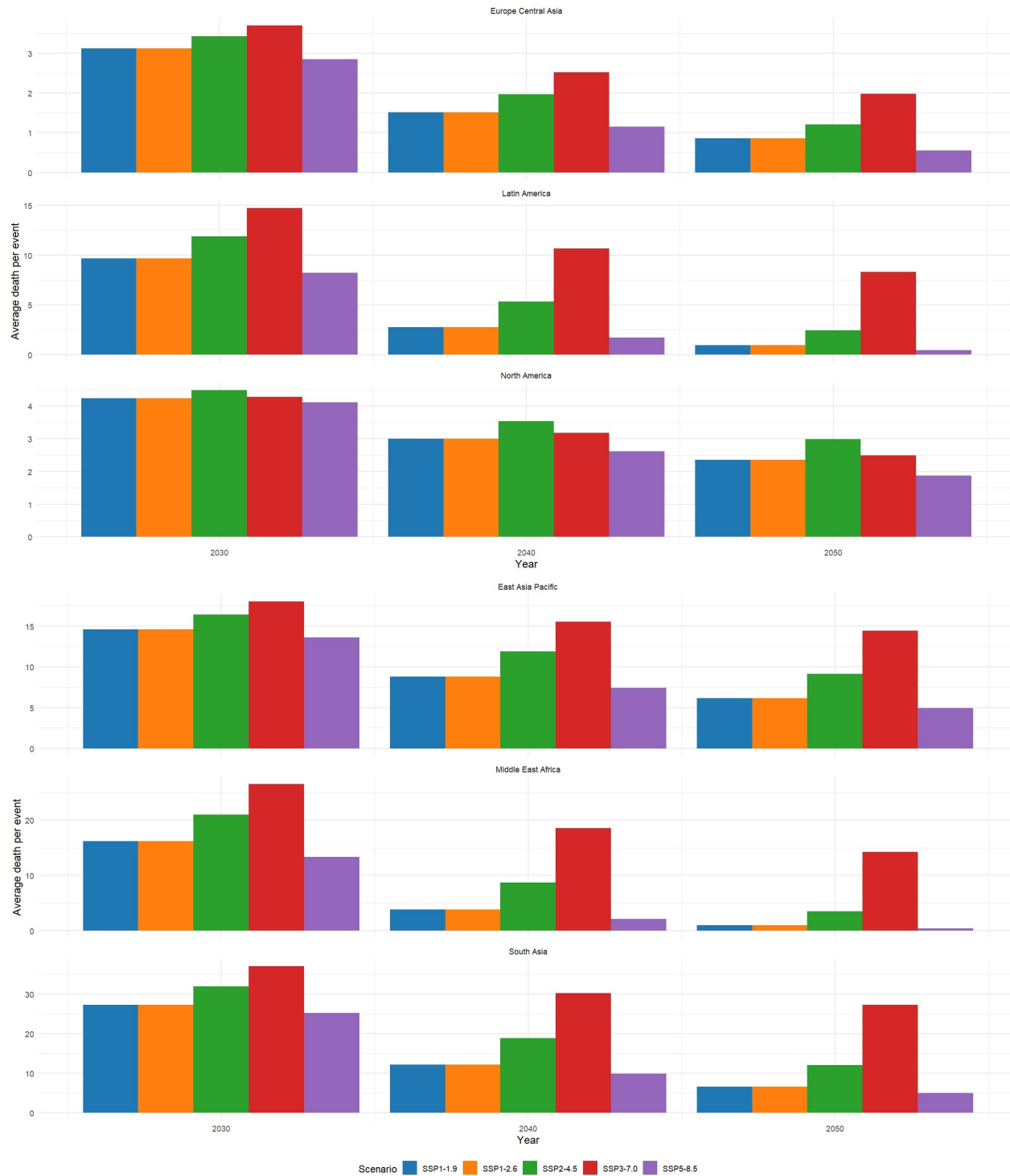


Figure 22. Projection number of death per flood event in 2030, 2040, and 2050

### 4.3 Annual Deaths

#### Projections

In Figure 23, the projections of the annual deaths for each region are presented based on the SSP scenarios. These numbers were determined using the formula given in Equation 12. For a more in-depth examination of these predictions, one may refer to Tables C1 through C5 found in Appendix C.

In the SSP1 (Sustainability) scenario, projections indicate a significant decline in annual deaths, nearing zero by 2040. The SSP2 (Middle of the Road) and SSP3 (Regional Rivalry) scenarios also forecast a notable reduction in deaths, albeit less pronounced than in SSP1. Conversely, the SSP5 (Fossil-fueled Development) scenario predicts slight decreases in deaths by 2040, but by 2050, the numbers approach those observed in 2011-2020. Notably, while enhanced GDP growth in the SSP5 scenario decreases individual flood severity, the rise in CO<sub>2</sub> levels correlates with a spike in flood occurrences. Consequently, the predicted annual deaths in 2050 are projected to be roughly equivalent to current levels.

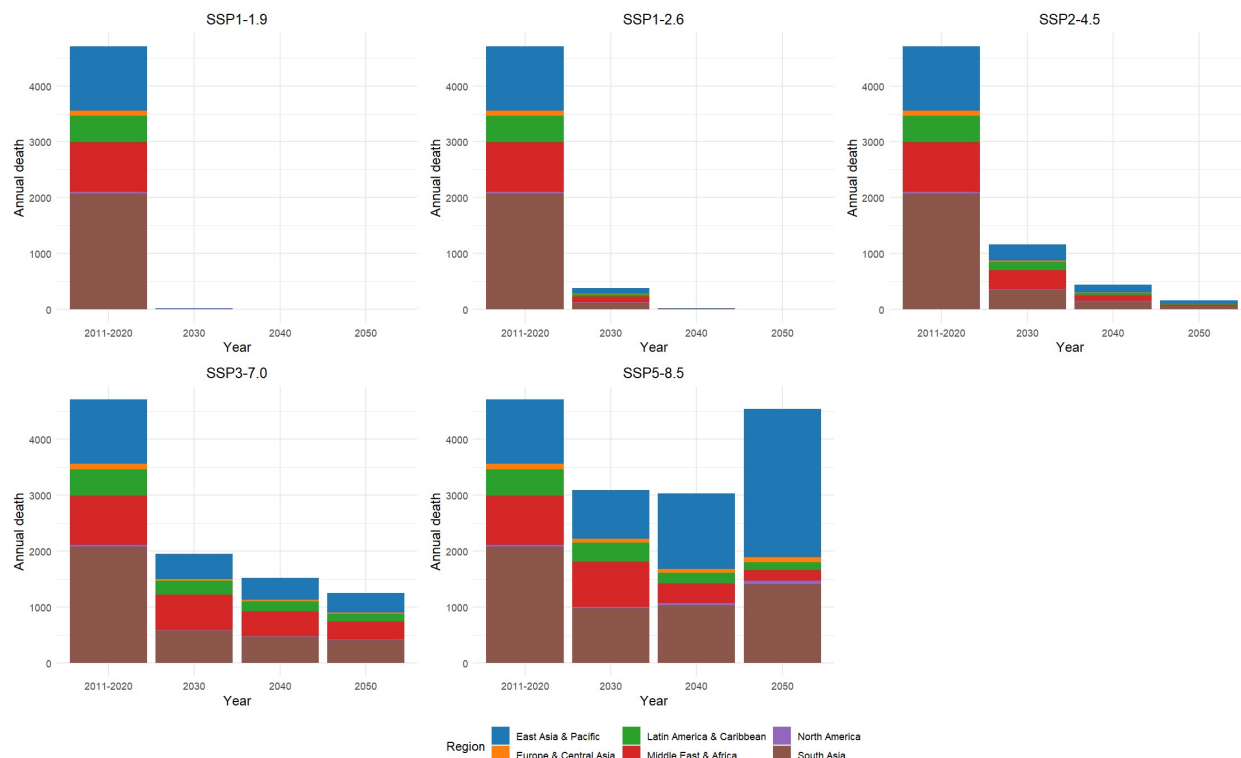


Figure 23. Projection annual death in 2030, 2040, and 2050

## 4.4 World

### Projections

When predicting on a global scale, we use the bootstrap method. In this methodology, we generate simulated data representing both the frequency of disasters and the death toll for each disaster category across various regions. These figures are then aggregated to produce the global projections. Notably, to account for the variability inherent in the predictions, we conduct 200 simulations. From these simulations, we calculate the variability range for both global disaster occurrences and the associated death toll. Specifically, we extract the 95% confidence interval from all these subsample simulations.

The charts in Figures 24, 25, and 26 display the estimated global predictions for flood frequency, the number of deaths expected per each flood event, and the total number of deaths, respectively, in the years 2030, 2040, and 2050, across five different SSP scenarios.

The projections concerning the frequency of flood occurrences (illustrated in Figure 24), which are inherently sensitive to shifts in CO<sub>2</sub> emissions, reveal declines in projected frequencies. Notably, all scenarios except SSP5 exhibit such downward trends, with the SSP1-1.9 scenario displaying the most pronounced reduction. This aligns with the SSP1-1.9 scenario's optimistic nature, as this trend gradually leads to an almost complete absence of flood events by 2050. This observation emphasizes the scenario's core assumption that CO<sub>2</sub> emissions will gradually decrease and eventually reach zero by 2050. Conversely, at the opposite end of the spectrum, due to the elevated levels of CO<sub>2</sub> emissions within the SSP5-8.5 Scenario, the projected global flood frequency is expected to surge by more than tenfold. It is of significance to highlight that the confidence interval established at a 95% confidence level exhibits a relatively compact range (approximately  $\pm 30\%$ ), indicative of the substantial confidence in the predictive model. This observation is underpinned by the relatively high value of the Adjusted R-squared derived from the estimation model, standing at 58.3% as reported in Equation 8.

The forecasts for global loss severity per flood incident, as illustrated in Figure 25, are significantly influenced by GDP growth. As evidenced in Figure 14, GDP projections exhibit an upward trend, albeit at varying magnitudes across different scenarios. Correspondingly,

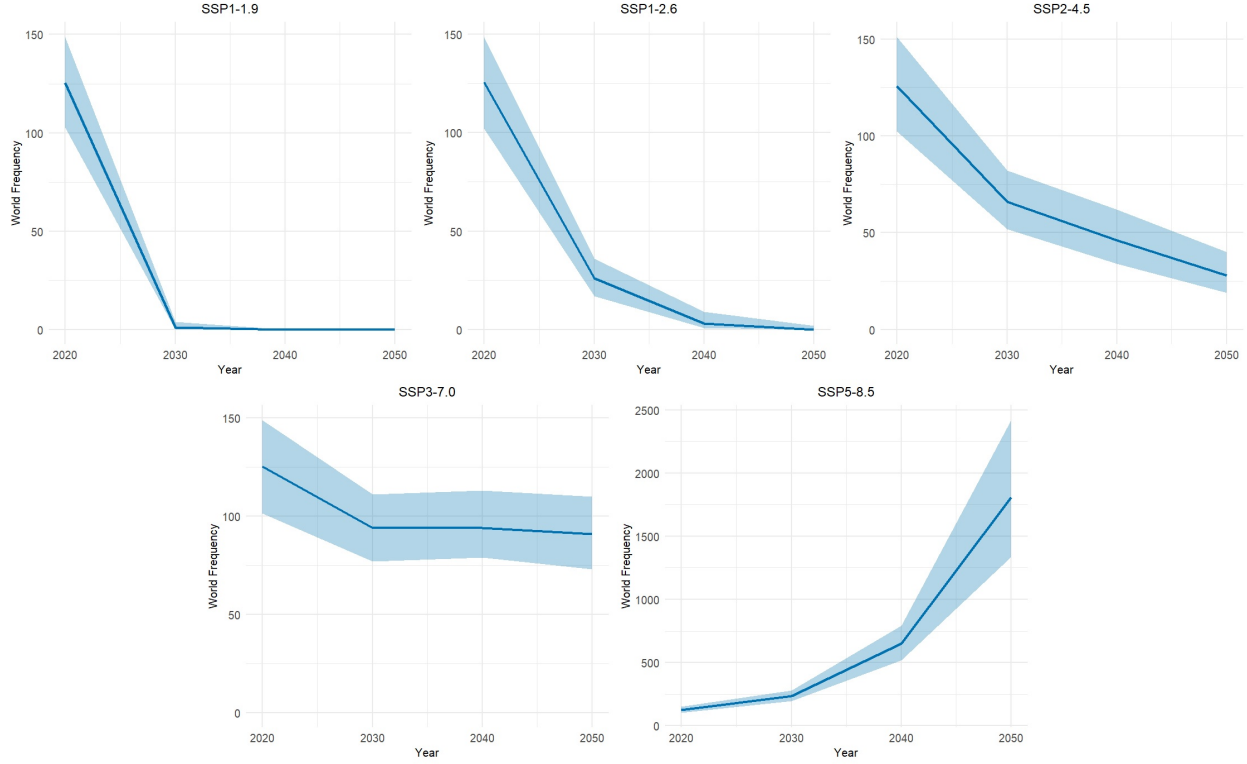


Figure 24. Projected Global Flood Frequency in 2030, 2040, and 2050 with 95% Confidence Interval

our results demonstrate a consistent decline in loss severity per flood incident across all scenarios. This pattern suggests that as countries attain greater economic prosperity, they enhance their capacity for effective disaster risk management, thereby reducing the severity of losses for each event.

It is important to highlight that the GDP growth projections for both SSP1-1.9 and SSP1-2.6 scenarios are the same. Consequently, under theoretical circumstances, one would anticipate identical projections for these two scenarios, as shown in Figure 22. Nonetheless, based on our simulation results, the occurrence of a flood event under the SSP1-1.9 scenario is unlikely to happen. In such an instance, the absence of flood events would translate to *n/a* average death toll. For the purposes of our simulation, *n/a* values are treated as zero, explaining why the results for the SSP1-1.9 scenario appear lower.

Regarding global annual deaths illustrated in Figure 26, all scenarios exhibit a declining trend with the exception of the SSP5-8.5 scenario. For the SSP5-8.5 scenario, there is a marginal decrease in the years 2030 and 2040, followed by an upward trajectory in 2050.

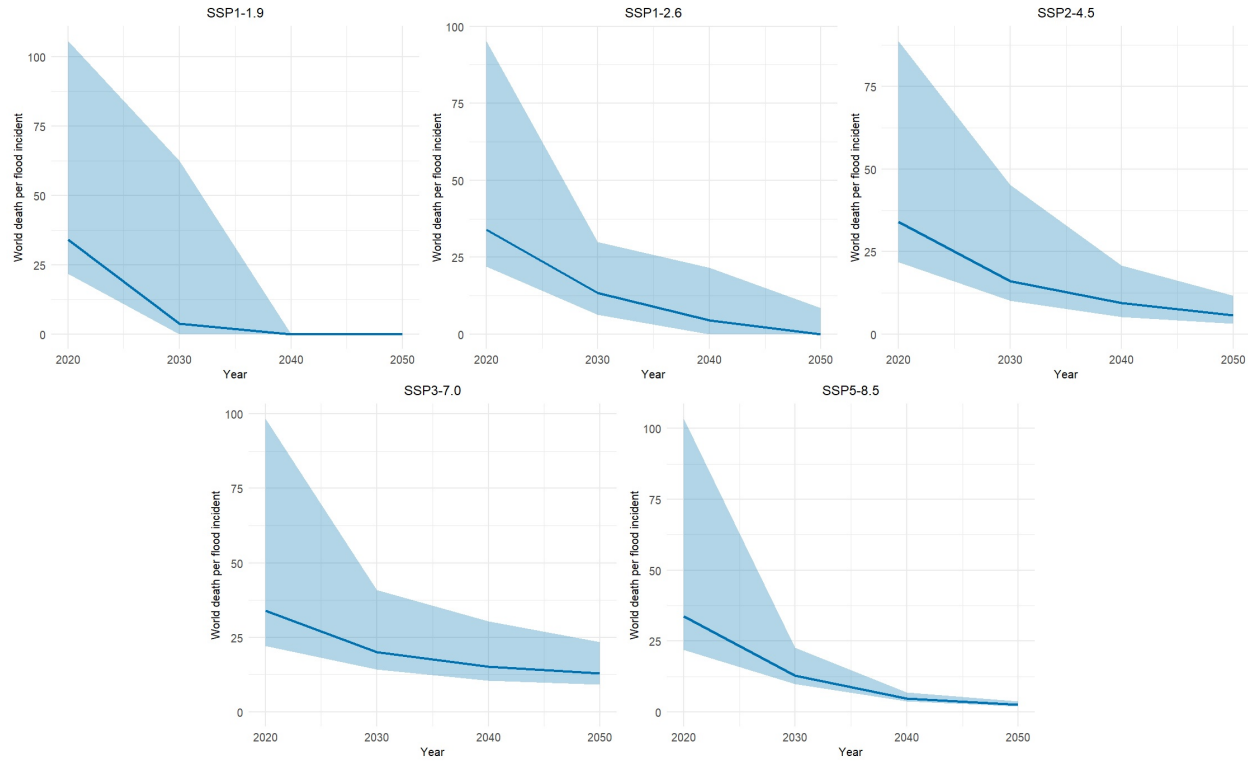


Figure 25. Projected Global Death per flood incident in 2030, 2040, and 2050 with 95% Confidence Interval

This observation underscores a nuanced understanding: while the SSP5-8.5 scenario registers the most significant reduction in loss severity per flood event, an anticipated surge in flood frequency seems to counterbalance this decline. Consequently, the projected annual death toll from flood events in 2050 under this scenario remains relatively unchanged from the present figures.

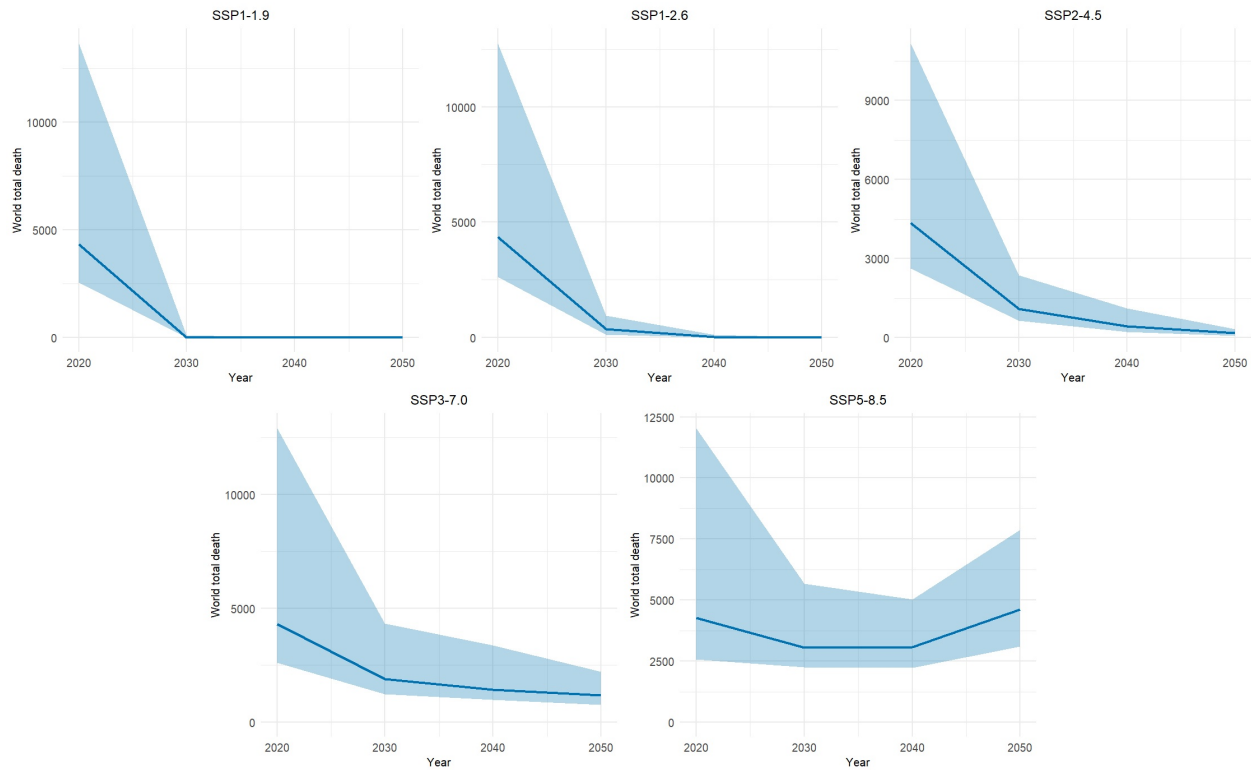


Figure 26. Projected Total Annual Global Deaths for 2030, 2040, and 2050 with a 95% Confidence Interval

## 5. Conclusion, Limitation, and Future Research

### 5.1 Conclusion

In conclusion, this thesis examines the link between climate-related disasters and death tolls, focusing on floods. Employing quantitative analysis using data from EM-DAT, World Bank, and IPCC databases, the study finds floods to be highly climate events causing substantial human losses. The research employs IPCC projections for CO<sub>2</sub> emissions, GDP, and population to forecast flood frequency and severity across climate scenarios (SSPs). Four key findings emerge:

(1) Flood Frequency: The Poisson model reveals CO<sub>2</sub> emissions and flood frequency positive correlation. Specifically, a 1% increase in CO<sub>2</sub> emissions corresponds to a percentage increase in flood frequency. Projections indicate declining trends except SSP5-8.5, which surges due to CO<sub>2</sub> levels. SSP1-1.9 sees the greatest reduction.

(2) Average Death per Flood Event: The Generalized Pareto Distribution (GPD) model exposes a significant negative link between GDP and flood severity, suggesting higher GDP regions experience milder floods. The relationship is robust at a 99.9% confidence level. Loss severity lessens across all scenarios, especially in SSP5-8.5. For instance, the expected number of deaths per event in South Asia averaged 99.2 during the 2011-2020 period, sharply decreasing to 5.0 by 2050 under the SSP5-8.5 scenario. The smallest reduction is observed in the SSP3-7.0 scenario.

(3) Annual Deaths: Projections anticipate reduced deaths across scenarios except for SSP5-8.5, which sees a brief dip followed by a rise due to CO<sub>2</sub> levels. SSP1-1.9 predicts substantial reduction.

(4) Global Perspective: Flood trends correlate regionally with CO<sub>2</sub> shifts. Projections show a decline except for SSP5-8.5, which surges. Confidence interval is narrow ( $\pm 30\%$ ). Global losses per event tie to GDP growth. Loss reduction is consistent across scenarios. Annual deaths fall except SSP5-8.5, with a temporary drop and 2050 increase.

Implications cover the areas of effective risk reduction, early warning systems, and vulnerability research, especially in developing nations. This thesis enriches climate disaster

literature, offering insights into flood management challenges, mitigation, and future research directions.

## 5.2 Limitation

The thesis presents distinct limitations:

1. **Regional Classification:** One limitation of this thesis relates to the regional classification of the 'Middle East and Africa'. At the beginning of the study, our aim was to separate this region into two distinct regions: 'Middle East and North Africa' (MENA) and 'Sub-Saharan Africa', based on the World Bank's regional classification. Such a division seemed fitting given the distinct socio-economic characteristics that set the two regions apart. However, a challenge arose when using the projection data from IPCC, which does not differentiate between North Africa and Sub-Saharan Africa. As a result, to overcome this issue, we combined the Middle East and Africa into one region. We believe that this combination may lead to errors in our predictions. By merging such diverse regions, our analysis might miss important climatic and socio-economic differences crucial for accurate forecasting. Moreover, climate vulnerabilities, adaptive capacities, and exposure levels can be quite different between these regions. Using a single classification means there is a chance of making general statements that might not truly capture the specific conditions or challenges of each region, possibly resulting in reduced accuracy of our findings.
2. **Data Scarcity for North American Flood Events:** As observed in Section 2.5 EDA, we identify a challenge related to the frequency of flood events in North America. Notably, during the early years of our time series, from 1960 to 1980, flood occurrences in North America are markedly infrequent. This scarcity of data might escalate potential inaccuracies in the model due to the constrained sample size pertaining to flood events in that region.
3. **Bootstrap Simulation Method:** Another limitation we need to consider is our use of the bootstrap simulation method. While this approach is used to enhance

result accuracy, it is important to acknowledge its inherent limitation. To achieve even greater precision in our outcomes, an increased number of simulations would be advantageous. Unlike our current study, which encompasses the execution of 200 simulations, a larger quantity of simulations would be preferable. However, it is important to recognize that it also requires more computational power.

4. **Rebasement Challenges: The Implications of Using 2020 Data for Future CO2 and GDP Projections:** In this thesis, we use historical CO2 emission and GDP data up to the year 2020, designating the values from that year as our baseline figures. For future projections, to maintain consistency between the IPCC projections and our historical data, we adjust the IPCC figures to match the 2020 historical data. However, this presents a complication. The year 2020 was marked by an unprecedented event, the COVID-19 lockdown, during which many businesses ceased operations and people were mandated to remain at home. Consequently, both CO2 emissions and GDP for 2020 experienced significant declines. Such an event can be considered a rare occurrence, perhaps once in a century. It is clear that the 2020 projections from the IPCC did not factor in the implications of the COVID-19 lockdown. Therefore, by rebasing the projection numbers in the year 2020 to the 2020 actual data, there is a potential risk of underestimating future projections for both CO2 emissions and GDP.
5. **Omission of the Non-linear Relationship Between Income Levels and Vulnerability to Natural Disasters:** Thomas et al.[15] found that higher income initially increases vulnerability to natural disasters, particularly in growth-focused developing nations with insufficient disaster management. Yet, over time, this vulnerability decreases as economies bolster their resilience, reducing disaster risk. Our thesis does not further investigate this relationship.

### 5.3 Future Research

The study on the climate-related flood and death toll reveals the complexities introduced by various contributing elements. To enhance our understanding and provide a comprehensive perspective, several topics for further research are recommended:

1. **Segregation of Middle East and Africa:** Although this study combines both regions into one, it would be advantageous for subsequent research to delve into a more granular classification by differentiating between 'Middle East and North Africa' (MENA) and 'Sub-Saharan Africa'. This distinction is pivotal, considering the vast socio-economic and climatic variances between these regions. However, the main challenges will be formulating a methodology to segregate these regions within the IPCC projections, specifically for both CO<sub>2</sub> emissions and GDP per capita. Addressing this gap will provide a more comprehensive understanding, potentially leading to more accurate forecasts.
2. **Temporal Variation in Rebasement Data:** The COVID-19 pandemic significantly affected the data for 2020, making it an outlier in the historical dataset. To understand the genuine long-term implications of rebasement, one could perform a sensitivity analysis using data from adjacent years (e.g., 2019 or 2021) as alternative baseline figures. This would provide insights into how much impact a single extraordinary year has on the long-term projections and assess the robustness of using 2020 data.
3. **Modeling Non-linear Dynamics between Income Levels and Disaster Vulnerability:** As outlined in the limitation section, our study does not account for the non-linear relationship between income levels and vulnerability to natural disasters as described by Thomas et al.[15]. Future research should prioritize modeling this association, enabling a more refined understanding of vulnerability dynamics, especially in developing countries. This exploration will shed light on the adaptive strategies and potential pitfalls these countries may encounter during their growth trajectories.

# Appendices

## Appendix A: Expected Annual Frequency Projections

Year	East Asia & Pacific	Europe & Central Asia	Latin America & Caribbean	Middle East & Africa	North America	South Asia	Total
2011-2020	33.8	13.5	22.2	31.1	3.9	20.4	124.9
2030	0.3	0.2	0.3	0.3	0.1	0.2	1.4
2040	0.0	0.0	0.0	0.0	0.0	0.0	0.0
2050	0.0	0.0	0.0	0.0	0.0	0.0	0.0

Table A1. Expected Annual Flood Frequency Projections - SSP1-1.9

Year	East Asia & Pacific	Europe & Central Asia	Latin America & Caribbean	Middle East & Africa	North America	South Asia	Total
2011-2020	33.8	13.5	22.2	31.1	3.9	20.4	124.9
2030	6.7	3.1	4.8	6.3	1.1	4.5	26.5
2040	1.0	0.5	0.7	0.9	0.3	0.7	4.1
2050	0.1	0.1	0.1	0.1	0.0	0.1	0.4

Table A2. Expected Annual Flood Frequency Projections - SSP1-2.6

Year	East Asia & Pacific	Europe & Central Asia	Latin America & Caribbean	Middle East & Africa	North America	South Asia	Total
2011-2020	33.8	13.5	22.2	31.1	3.9	20.4	124.9
2030	17.4	7.4	11.8	16.1	2.3	11.0	66.2
2040	12.0	5.3	8.3	11.2	1.8	7.8	46.3
2050	7.3	3.3	5.1	6.8	1.2	4.8	28.5

Table A3. Expected Annual Flood Frequency Projections - SSP2-4.5

Year	East Asia & Pacific	Europe & Central Asia	Latin America & Caribbean	Middle East & Africa	North America	South Asia	Total
2011-2020	33.8	13.5	22.2	31.1	3.9	20.4	124.9
2030	25.2	10.3	16.8	23.3	3.1	15.6	94.2
2040	25.4	10.4	16.9	23.5	3.1	15.7	95.0
2050	24.4	10.0	16.3	22.6	3.0	15.2	91.4

Table A4. Expected Annual Flood Frequency Projections - SSP3-7.0

Year	East Asia & Pacific	Europe & Central Asia	Latin America & Caribbean	Middle East & Africa	North America	South Asia	Total
2011-2020	33.8	13.5	22.2	31.1	3.9	20.4	124.9
2030	65.5	24.4	41.6	59.8	6.5	37.9	235.7
2040	185.4	62.5	111.1	168.0	14.6	102.4	644.1
2050	532.6	161.5	305.3	480.8	32.9	280.4	1793.6

Table A5. Expected Annual Flood Frequency Projections - SSP5-8.5

## Appendix B: Expected Death toll per event Projections

Year	East Asia & Pacific	Europe & Central Asia	Latin America & Caribbean	Middle East Africa	North America	South Asia
2011-2020	34.0	7.1	21.1	28.9	6.6	99.2
2030	14.6	3.1	9.7	16.2	4.2	27.3
2040	8.8	1.5	2.8	3.8	3.0	12.2
2050	6.1	0.9	0.9	0.9	2.4	6.6

Table B1. Expected Death toll per event Projections - SSP1-1.9 and SSP1-2.6

Year	East Asia & Pacific	Europe & Central Asia	Latin America & Caribbean	Middle East Africa	North America	South Asia
2011-2020	34.0	7.1	21.1	28.9	6.6	99.2
2030	16.4	3.4	11.9	21.0	4.5	32.0
2040	11.9	2.0	5.4	8.7	3.5	18.9
2050	9.1	1.2	2.4	3.5	3.0	12.1

Table B2. Expected Death toll per event Projections - SSP2-4.5

Year	East Asia & Pacific	Europe & Central Asia	Latin America & Caribbean	Middle East Africa	North America	South Asia
2011-2020	34.0	7.1	21.1	28.9	6.6	99.2
2030	18.0	3.7	14.7	26.6	4.3	37.0
2040	15.5	2.5	10.7	18.6	3.2	30.2
2050	14.4	2.0	8.3	14.3	2.5	27.3

Table B3. Expected Death toll per event Projections - SSP3-7.0

Year	East Asia & Pacific	Europe Central Asia	Latin America & Caribbean	Middle East Africa	North America	South Asia
2011-2020	34.0	7.1	21.1	28.9	6.6	99.2
2030	13.6	2.9	8.2	13.4	4.1	25.3
2040	7.4	1.1	1.7	2.1	2.6	9.9
2050	4.9	0.6	0.4	0.4	1.9	5.0

Table B4. Expected Death toll per event Projections - SSP5-8.5

### Appendix C: Annual Death Projections

Year	East Asia & Pacific	Europe & Central Asia	Latin America & Caribbean	Middle East & Africa	North America	South Asia	Total
2011-2020	1150.8	95.6	468.5	887.4	26.3	2078.7	4707.4
2030	4.5	0.6	2.4	4.9	0.4	6.7	19.5
2040	0.0	0.0	0.0	0.0	0.0	0.0	0.0
2050	0.0	0.0	0.0	0.0	0.0	0.0	0.0

Table C1. Expected Annual Death Projections - SSP1-1.9

Year	East Asia & Pacific	Europe & Central Asia	Latin America & Caribbean	Middle East & Africa	North America	South Asia	Total
2011-2020	1150.8	95.6	468.5	887.4	26.3	2078.7	4707.4
2030	98.2	9.8	46.4	102.6	4.8	123.2	385.0
2040	8.5	0.8	2.1	3.6	0.7	8.5	24.2
2050	0.5	0.0	0.1	0.1	0.1	0.4	1.2

Table C2. Expected Annual Death Projections - SSP1-2.6

Year	East Asia & Pacific	Europe & Central Asia	Latin America & Caribbean	Middle East & Africa	North America	South Asia	Total
2011-2020	1150.8	95.6	468.5	887.4	26.3	2078.7	4707.4
2030	284.1	25.5	143.2	340.9	10.6	353.9	1158.2
2040	141.9	10.4	44.6	97.7	6.3	146.0	446.8
2050	65.4	4.0	12.3	23.5	3.6	58.3	167.1

Table C3. Expected Annual Death Projections - SSP2-4.5

Year	East Asia & Pacific	Europe & Central Asia	Latin America & Caribbean	Middle East & Africa	North America	South Asia	Total
2011-2020	1150.8	95.6	468.5	887.4	26.3	2078.7	4707.4
2030	447.8	38.2	251.0	621.4	13.3	579.2	1950.9
2040	387.6	26.3	183.8	437.0	10.0	471.6	1516.3
2050	345.0	19.8	138.2	322.1	7.6	411.6	1244.4

Table C4. Expected Annual Death Projections - SSP3-7.0

Year	East Asia & Pacific	Europe & Central Asia	Latin America & Caribbean	Middle East & Africa	North America	South Asia	Total
2011-2020	1150.8	95.6	468.5	887.4	26.3	2078.7	4707.4
2030	869.1	69.1	349.4	802.5	26.5	975.6	3092.2
2040	1345.4	70.8	193.8	350.8	38.0	1029.7	3028.5
2050	2653.0	89.5	138.1	195.5	61.6	1404.0	4541.6

Table C5. Expected Annual Death Projections - SSP5-8.5

## Bibliography

- [1] The International Institute for Applied Systems Analysis. *IIASA*. [https://previous.iiasa.ac.at/web/home/about/whatisiiasa/informationkit/iiasa-flyer\(1\).pdf](https://previous.iiasa.ac.at/web/home/about/whatisiiasa/informationkit/iiasa-flyer(1).pdf) Accessed: 2023-07-17.
- [2] Valérie Chavez-Demoulin, Eric Jondeau, and Linda Mhalla. *Climate-Related Disasters and the Death Toll*. Swiss Finance Institute Research Paper No. 21-63, Sept. 3, 2021.
- [3] Intergovernmental Panel on Climate Change (IPCC). *Water Cycle Changes*. In *Climate Change 2021 – The Physical Science Basis: Working Group I Contribution to the Sixth Assessment Report of the Intergovernmental Panel on Climate Change* (pp. 1055-1210). Cambridge University Press, 2023.
- [4] The Intergovernmental Panel on Climate Change (IPCC). *IPCC FACTSHEET What is the IPCC?*. Accessed: 2023-07-16. 2021. URL: [https://www.ipcc.ch/site/assets/uploads/2021/07/AR6\\_FS\\_What\\_is\\_IPCC.pdf](https://www.ipcc.ch/site/assets/uploads/2021/07/AR6_FS_What_is_IPCC.pdf).
- [5] United Nations Office for Disaster Risk Reduction (UNDRR). *Disaster risk reduction in the least developed countries*. Accessed: 2023-07-20. United Nations, Mar. 8, 2023. URL: <https://www.unrr.org/disaster-risk-reduction-least-developed-countries>.
- [6] Organisation for Economic Co-operation and Development. *Purchasing power parities (PPP)*. Accessed: 2023-07-16. URL: <https://data.oecd.org/conversion/purchasing-power-parities-ppp.htm>.
- [7] World Bank Group. *Disaster Risk Management Overview*. <https://www.worldbank.org/en/topic/disasterriskmanagement/overview> Accessed: 2023-07-17. World Bank, 2021.
- [8] Core Writing Team H. Lee and J. Romero (eds.) *IPCC, 2023: Climate Change 2023: Synthesis Report. A Report of the Intergovernmental Panel on Climate Change. Contribution of Working Groups I, II and III to the Sixth Assessment Report of the Intergovernmental Panel on Climate Change*. IPCC, Geneva, Switzerland, (in press), 2023.
- [9] Pablo Rosado Hannah Ritchie Max Roser. *CO<sub>2</sub> and Greenhouse Gas Emissions*. <https://ourworldindata.org/co2-and-greenhouse-gas-emissions> Accessed: 2023-07-16. 2020.
- [10] United Nations. *Causes and Effects of Climate Change*. <https://www.un.org/en/climatechange/science/causes-effects-climate-change> Accessed: 2023-07-26. United Nations.

- [11] Brian C. O'Neill et al. *The Scenario Model Intercomparison Project (ScenarioMIP) for CMIP6*. Geoscientific Model Development, 9(9), 3461–3482, 2016. URL: <https://doi.org/10.5194/gmd-9-3461-2016>.
- [12] CRED - Centre for Research on the Epidemiology of Disasters. *EM-DAT - The international disaster database*. Accessed: 2023-07-08. 2023. URL: <https://www.emdat.be/>.
- [13] Centre for Research on the Epidemiology of Disasters United Nations Office for Disaster Risk Reduction. *Poverty and Death: Disaster and Mortality 1996-2015*. 2016.
- [14] Keywan Riahi, Edward Byers, and Volker Krey. *AR6 Scenario Explorer and Database*. <https://iiasa.ac.at/models-tools-data/ar6-scenario-explorer-and-database>. 2023.
- [15] Vinod Thomas, Jose Ramon G Albert, and Rosa T Perez. *Climate-Related Disasters in Asia and the Pacific*. 2013.
- [16] Detlef Van Vuuren, Elke Stehfest, and David Gernaat. *THE 2021 SSP SCENARIOS OF THE IMAGE 3.2 MODEL*. PBL Netherlands Environmental Assessment Agency, Oct. 2021.